
FOUNDATION MODELS FOR ELECTROCARDIOGRAMS

A PREPRINT

Junho Song*, Jong-Hwan Jang, Byeong Tak Lee, DongGyun Hong,
Joon-myung Kwon, and Yong-Yeon Jo*

AI Group
Medical AI Co., Ltd.
Seoul, Republic of Korea
{jhsong*, jangood1122, bytaklee, dghong, cto, yy.jo}*@medicalai.com

ABSTRACT

Foundation models, enhanced by self-supervised learning (SSL) techniques, represent a cutting-edge frontier in biomedical signal analysis, particularly for electrocardiograms (ECGs), crucial for cardiac health monitoring and diagnosis. This study conducts a comprehensive analysis of foundation models for ECGs by employing and refining innovative SSL methodologies—namely, generative and contrastive learning—on a vast dataset of over 1.1 million ECG samples. By customizing these methods to align with the intricate characteristics of ECG signals, our research has successfully developed foundation models that significantly elevate the precision and reliability of cardiac diagnostics. These models are adept at representing the complex, subtle nuances of ECG data, thus markedly enhancing diagnostic capabilities. The results underscore the substantial potential of SSL-enhanced foundation models in clinical settings and pave the way for extensive future investigations into their scalable applications across a broader spectrum of medical diagnostics. This work sets a benchmark in the ECG field, demonstrating the profound impact of tailored, data-driven model training on the efficacy and accuracy of medical diagnostics.

Keywords Biosignal process · Foundation model · Generative learning · Contrastive learning · Electrocardiogram

1 Introduction

Electrocardiograms (ECGs) are essential bio-signals that record the heart's electrical activity, providing critical information about heart rhythm, strength, timing, and beat rate. These signals play a pivotal role in diagnosing heart diseases, detecting abnormalities that may indicate conditions such as myocardial infarction, arrhythmias, and other cardiac disorders. Analyzing ECGs is crucial for effective diagnosis and treatment, making advancements in this field highly impactful.

Deep Neural Networks (DNNs) have emerged as powerful tools for analyzing ECG data, capable of performing various tasks such as prediction, classification, and denoising. However, two significant challenges hinder their utilization. Firstly, ECG data is sensitive medical information that requires strict privacy protection, leading to a relative scarcity of available data. Secondly, the low incidence of certain heart diseases results in insufficient curated ECG datasets with annotated medical labels to effectively train DNNs.

Researchers have adopted foundation models with Self-Supervised Learning (SSL) to address these challenges, showing great promise in various fields, including natural language processing (Devlin et al., 2018; Achiam et al., 2023), computer vision (Chen et al., 2020; He et al., 2022), and speech recognition (Baeviski et al., 2020). In the context of ECG analysis, foundation models can generalize from unlabeled data and be fine-tuned with minimal labeled data, making them highly flexible and efficient.

Foundation models with SSL offer several key benefits:

*Corresponding Author

- **Reduced Need for Labeled Data:** SSL requires only unlabeled data to train foundation models, learning robust representations without the need for extensive labeled datasets.
- **Enhanced Accuracy and Efficiency:** These models can be fine-tuned for specific downstream tasks, resulting in improved accuracy and faster convergence compared to training models from scratch.
- **Resource Efficiency:** Since foundation models are pre-trained, fine-tuning them requires fewer computational resources, making the process more efficient.

The success of foundation models hinges on effective pre-training, which relies heavily on SSL methods. Two main streams of SSL are widely adopted: Contrastive Learning (CL) and Generative Learning (GL). CL enhances the model’s ability to distinguish between similar and dissimilar instances by bringing positive pairs closer and pushing negative pairs apart in the representation space. GL, on the other hand, focuses on reconstructing data by masking parts of the input, thereby improving the model’s ability to predict missing information (Lai et al., 2023; Wang et al., 2024; Chien et al., 2022; Na et al., 2024).

While promising, the application of foundation models for ECGs is still in its early stages. There is a need for extensive investigation into various aspects, such as representation schemes, SSL methods, and practical applications, to fully realize their potential. Our study aims to guide the development of foundation models for ECGs using a large-scale dataset of over 1.1 million samples. We investigate the models from three perspectives:

- **Representation scheme:** Analyzing the architectural design based on the Vision Transformer (ViT (Dosovitskiy et al., 2020)) to customize it for the unique characteristics of ECG data.
- **SSL methods:** Evaluating different SSL methodologies, including contrastive, generative, and hybrid approaches, to determine the most effective strategy for ECG data representation.
- **Practical applications:** Validating the efficacy of these models in real-world scenarios characterized by low incidence rates and restricted data availability.

Our contributions include:

- **Large-Scale Pre-Training:** To the best of our knowledge, this is the first work using a large-scale dataset to pre-train foundation models on ECG data.
- **Hybrid SSL Framework:** Introducing a novel combination of SSL techniques for foundation models of ECGs.
- **Guidance for Foundation Models:** Providing extensive insights through the comprehensive analysis into the performance of ECG foundation models using various SSL methods.

The findings of this study are expected to significantly enhance the application of SSL-enhanced foundation models in ECG classification tasks, providing a robust framework for future research and practical implementations in clinical settings.

2 Related Work

The advent of foundation models has revolutionized various fields by leveraging large-scale, unlabeled datasets to produce versatile and robust data representations. These representations enable models to adapt efficiently to specific downstream tasks with minimal reliance on labeled data, significantly enhancing performance and efficiency. In the realm of bio-signal analysis, particularly ECGs, the application of foundation models enhanced by Self-Supervised Learning (SSL) techniques has shown immense promise (Abbaspourazad et al., 2024; Yue et al., 2022).

2.1 Advanced Self-Supervised Learning Techniques for Foundation Models

Foundation models utilize advanced SSL techniques during their pre-training phase to learn meaningful data representations without direct supervision. These techniques are crucial for enabling versatile applications in subsequent task-specific training:

- **Contrastive Learning (CL):** CL improves a model’s ability to form embeddings by bringing similar instances closer in the embedding space while pushing dissimilar instances apart. This is typically achieved using a contrastive loss function, such as InfoNCE, which helps the model develop rich, semantically meaningful representations from unlabeled data. CL has been successfully applied across various domains, enhancing model performance on downstream tasks by improving the quality of learned representations (Chen et al., 2020).

- **Generative Learning (GL):** GL techniques, such as Masked AutoEncoders (MAE), challenge models to reconstruct obscured segments of input data. This process strengthens the model’s capacity to intuit and regenerate missing data components; fostering a deeper understanding of complex data patterns. GL has been particularly effective in applications like image and natural language processing, where it aids in denoising and anomaly detection (He et al., 2022; Dosovitskiy et al., 2020).
- **Hybrid Learning (HL):** HL combines the strengths of both CL and GL, leveraging the discriminative power of CL and the reconstructive ability of GL. This synergistic approach has shown promising results in domains such as computer vision and holds significant potential for ECG analysis and other medical tasks. By balancing the advantages of both methods, HL aims to create robust and flexible data representations (Huang et al., 2023).

2.2 Pioneering Applications of SSL in Bio-Signal Analysis

SSL methodologies have been increasingly adapted for bio-signal analysis, particularly in ECG, demonstrating substantial improvements in model accuracy and generalizability:

- **Diverse Approaches to ECG Analysis:** SSL has been instrumental in developing deep multi-task learning frameworks that significantly enhance emotion recognition from ECG signals, achieving state-of-the-art classification results. These frameworks illustrate the ability of SSL to capture complex physiological patterns inherent in ECG data (Sarkar and Etemad, 2020).
- **Innovative ECG Classification Techniques:** Techniques such as U-ResNet-based SSL have shown meaningful improvements in ECG classification accuracy, underscoring the utility of SSL in clinical diagnostics. These methods leverage SSL pre-training to refine models, leading to better performance compared to traditional supervised approaches (Gedon et al., 2021).
- **Addressing Data Challenges:** SSL methods have been employed to overcome challenges like label imbalance and data scarcity in ECG datasets. Self-supervised pre-training has demonstrated superior performance in handling complex bio-signal datasets, highlighting the effectiveness of SSL in managing the inherent challenges of ECG data (Liu et al., 2021).
- **Lead-agnostic Learning Models:** Developing SSL methods that are agnostic to ECG leads and capable of learning both local and global features has shown improved adaptability and performance on downstream tasks. These approaches enhance the flexibility and generalizability of SSL in medical applications, making them valuable for diverse clinical scenarios (Oh et al., 2022).
- **Non-contrastive Learning for ECG:** The introduction of non-contrastive SSL approaches, which do not rely on data augmentation or negative pairs, offers a novel pathway for SSL application in bio-signal processing. These methods provide an alternative to traditional contrastive techniques, simplifying the training process and potentially improving model performance (Atienza et al., 2023).

2.3 Research Goals

Despite the promising results and growing adoption of SSL for bio-signal generalization, such as ECG, EEG, and PPG, there remains a significant gap in comprehensive implementation strategies for applying foundation models using diverse SSL frameworks in real-world healthcare settings. The existing literature often revolves around closed datasets and controlled experimental conditions, which may not accurately replicate the complexities encountered in practical environments (Na et al., 2024, Abbaspourazad et al., 2024, Liu et al., 2024).

Our research aims to bridge these gaps by providing detailed and empirically supported guidance on pre-training foundation models. We meticulously evaluate these models across a broad spectrum of architectural designs and SSL methodologies, enhancing their efficacy for bio-signal applications such as ECG. By extending our investigations to include a wide range of real-world applications, we seek to refine these foundation models to better suit clinical needs, thereby advancing their readiness for broader healthcare applications and facilitating significant technological advancements in medical practice.

3 Study Procedure

Our study’s methodology unfolds through a meticulously structured sequence of steps, aiming to provide a comprehensive evaluation of foundation models for ECG classification. The process includes data preparation, model training, thorough evaluation, and analysis, ensuring a robust framework for developing and assessing the performance of these models. The entire procedure of our study is illustrated in Figure 1.

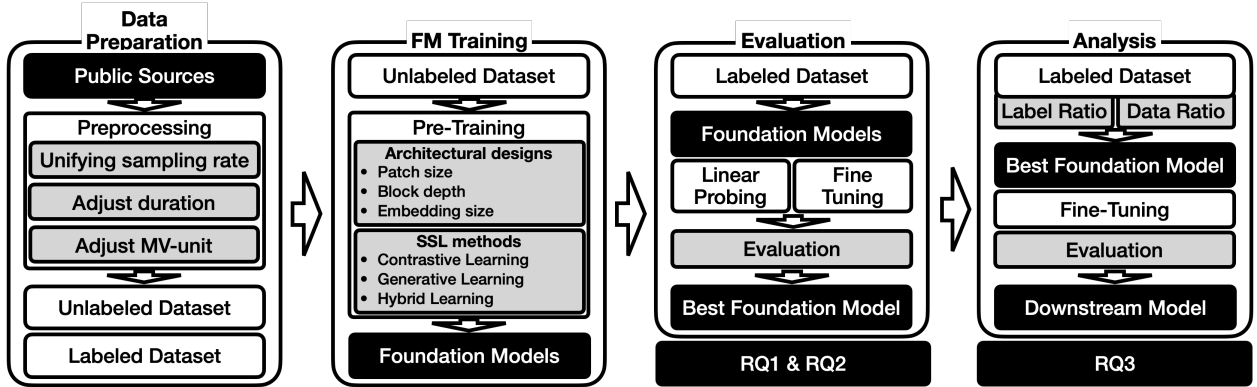


Figure 1: Study procedure

3.1 Data preparation

We utilized two types of datasets: unlabeled and labeled. The unlabeled dataset, presented in Table 1, was compiled from five public repositories, MIMIC (Johnson et al., 2016), CODE15 (Ribeiro et al., 2021), BIOBANK (Sudlow et al., 2015), SAMI (Ribeiro et al., 2021), and IKEM (Sejak et al., 2023), to ensure demographic fairness by including data collected from various continents. This dataset encompasses a total of 1,291,868 ECG samples from 442,736 distinct patients, aiding in mitigating potential biases and enhancing the generalizability of the study results.

Table 1: Summary of the unlabeled dataset.

	Category	Name	Demographic Information		Statistics				
			#Patients	Country	#Sample	#Leads	MV-unit	Duration (s)	Sample rate (Hz)
Unlabeled	Public	MIMIC	161,352	USA	800,035	12	0.005	10	500
		CODE15	233,770	USA	341,292	12	1	10	400
		BIOBANK	15,365	UK	50,780	12	0.005	10	500
		SAMI	1,959	Brazil	1,631	12	1	10	400
		IKEM	30,290	Czech Republic	98,130	12	0.004	10	500

For the classification tasks, we employed labeled datasets, specifically utilizing ECGs from the PTB-XL dataset outlined in Table 2. This dataset includes super-classes: MI (Myocardial Infarction), STTC (ST/T change), CD (Conduction Disturbance), and HYP (Hypertrophy). These super-classes were chosen to reflect the diverse morphologies, features, and rhythmic patterns inherent in ECG data, providing a robust framework for assessing the efficacy of our foundation models. The dataset comprises a total of 21,265 ECG samples collected from 8,000 patients.

Table 2: Summary of the labeled dataset.

	Category	Name	Demographic Information			Statistics				
			#Patients	Label	Case ratio	#Sample	#Leads	Length	Duration (s)	Sample rate (Hz)
Labeled	Public	PTB-XL	5,466	MI	0.2524	6,886	12	5,000	10	500
			5,107	STTC	0.2382	5,788	12	5,000	10	500
			4,897	CD	0.2211	5,772	12	5,000	10	500
			2,648	HYP	0.1209	2,819	12	5,000	10	500

Before analysis, all data underwent a standardization process to account for inherent variances in sample rates, measuring durations, and MV-units among different datasets. To standardize our comparisons and maintain consistency across analyses, we adjusted the sample rate to 250 Hz, the measurement duration to 10 seconds, and the MV-units to 1.0, rendering each ECG signal in our dataset to consist of a 2500 length per lead.

3.2 Model Training

3.2.1 Foundation models

We adopt widely recognized Self-Supervised Learning (SSL) methodologies to pre-train our foundation models, specifically focusing on Generative Learning (GL), Contrastive Learning (CL), and Hybrid Learning (HL). These models incorporate the Vision Transformer (ViT) (Dosovitskiy et al., 2020) as the primary architectural backbone,

modified with a one-dimensional convolution projection layer specifically tailored for embedding ECG signals (Woo et al., 2023). The comprehensive architecture of our foundation models, which effectively combines these innovative self-supervised learning strategies.

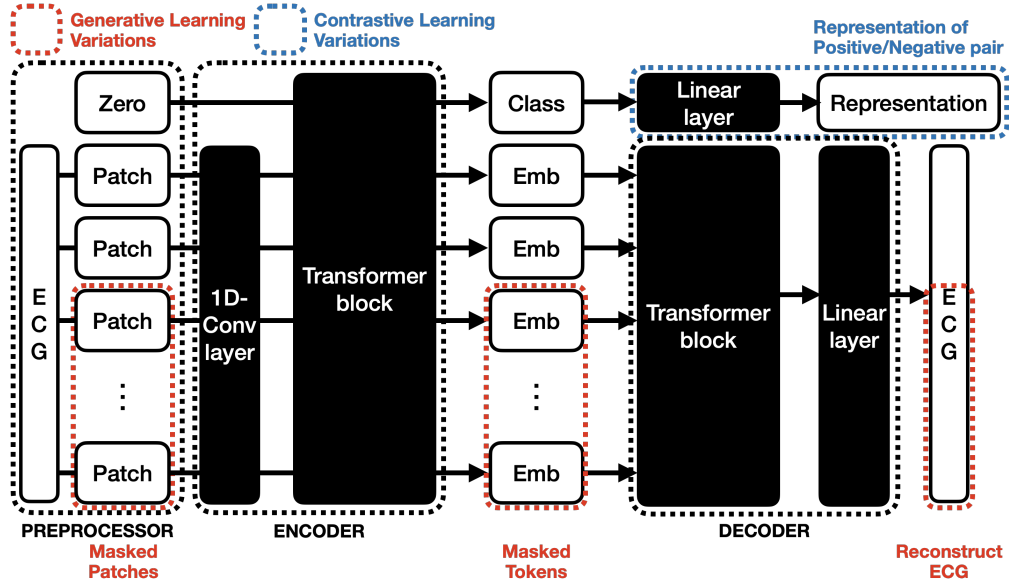


Figure 2: Structure of foundation models

Figure 2 illustrates the overall structure: the preprocessor divides ECG signals into patches, the encoder extracts features and understands global contextual relationships, and the decoder reconstructs the original ECG signals from the embeddings. By integrating these self-supervised learning methodologies, especially the pioneering HL approach, the foundation models effectively capture complex patterns in ECG data, significantly improving their utility in various downstream tasks, such as classification and prediction, and setting a new benchmark in the field.

In the training of foundation models for ECG analysis, we employ three primary self-supervised learning (SSL) methodologies: Contrastive Learning (CL), Generative Learning (GL), and Hybrid Learning (HL), each with a specific focus and procedure. As depicted in Figure 2, the preprocessor divides the input ECG signals into smaller patches using a one-dimensional convolution projection layer.

For CL, these patches are augmented to create different views, forming positive and negative pairs. The encoder, consisting of 1D-Convolutional layers and a Transformer block, processes these patches to extract features and generate embeddings. The contrastive learning objective is to bring the embeddings of positive pairs closer while pushing the embeddings of negative pairs apart, achieved using the contrastive loss function (InfoNCE loss):

$$L_{CONT} = -\log \frac{\exp(\mathbf{z}_i \cdot \mathbf{z}_j / \tau)}{\sum_{k=0}^N \exp(\mathbf{z}_i \cdot \mathbf{z}_k / \tau)} \quad (1)$$

where z_i and z_j are the embeddings of the positive pair, τ is a temperature parameter, and N is the number of negative samples. During training, the encoder weights are updated to minimize this loss, enhancing the model’s ability to distinguish between similar and dissimilar ECG signals.

For GL, the preprocessor randomly masks a portion of the patches, creating incomplete ECG inputs. The encoder processes the unmasked patches, and the resulting embeddings are input into the transformer decoder, which aims to reconstruct the original ECG signals. The generative learning objective is to minimize the reconstruction loss, quantified using the mean absolute error (MAE):

$$L_{RECON} = \sum_{i=1}^N |x_i - y_i| \quad (2)$$

where x_i is the original signal and y_i is the reconstructed signal. The encoder and decoder weights are updated to minimize this loss during training, improving the model’s ability to predict missing information.

Hybrid Learning (HL) is a novel approach applied for the first time in training foundation models for ECG data in this study. It combines the strengths of both CL and GL to create a more robust and versatile learning framework. The preprocessor creates both augmented pairs for CL and masked patches for GL. The encoder processes the unmasked patches, generating embeddings used in both the contrastive and generative learning objectives. The total hybrid loss combines the contrastive loss and the reconstruction loss:

$$L_{HYBRID} = L_{RECON} + L_{CONT_{Patient}} + L_{CONT_{Sample}} \quad (3)$$

where $L_{CONT_{Patient}}$ and $L_{CONT_{Sample}}$ are the contrastive losses calculated at the patient and sample levels, respectively. The encoder and decoder weights are updated to minimize this combined loss, leveraging the benefits of both learning strategies to enhance the model’s representation capabilities. This hybrid approach not only maximizes the representational power of the models but also ensures they are adept at capturing and categorizing complex patterns within ECG data.

3.2.2 Downstream models

After pre-training the foundation models using SSL, we employed two downstream learning strategies to assess their performance: linear probing and fine-tuning.

Linear Probing: Linear probing involves freezing the weights of the pre-trained foundation model and adding a linear classifier on top of its output layer. This linear classifier is trained using the labeled ECG dataset, evaluating the quality of the learned representations without updating the pre-trained model’s weights. This approach provides insights into how well the foundation model’s pre-trained features can be used for classification tasks.

Fine-Tuning: Fine-tuning involves updating the weights of the entire model, including both the pre-trained foundation model and the newly added linear classifier. This step allows the model to adapt more specifically to the classification tasks using the labeled dataset. Fine-tuning typically results in better performance than linear probing, as it adjusts the pre-trained features to better fit the specific characteristics of the labeled data.

3.3 Evaluation

The evaluation of these downstream models is conducted from two critical viewpoints: optimization and applicability.

Optimization: We scrutinize the parameters utilized during the pre-training phase of the foundation models, focusing on their architectural designs and SSL methodologies, to determine their impact on the representation of ECG data. The evaluation includes: Impact of Patch Size, Influence of Block Depth, Role of Embedding Size.

Applicability: We assess the practical effectiveness of these models in ECG classification tasks, considering variables such as data availability and case ratios. This involves validating the efficacy of these models in real-world scenarios characterized by low incidence rates and restricted data availability.

3.4 Analysis

3.4.1 Research Questions

Our research endeavors to elucidate the potential of self-supervised learning (SSL) in the context of electrocardiogram (ECG) modeling through foundation models. It systematically addresses several pivotal research questions designed to deepen our understanding of model development and integration within practical settings:

RQ1. What architectural designs of foundation models are most effective for capturing the nuanced semantics of ECG?

The foundation model is pivotal in generalizing electrocardiogram (ECG) data effectively. Determining the most suitable architectural designs to capture diverse ECG signal features—including beat rate, *pqrst* values, morphological attributes, and temporal correlations—is critical. We conducted an extensive grid search to investigate the impact of key parameters such as patch size, depth, and embedding size on data representation. This search involved testing patch sizes of 250, 125, and 60; depths of 2, 4, and 8; and embedding sizes of 256, 512, and 1024, with embedding sizes set to half that of the encoders. This methodical exploration aims to identify the architectural designs that most accurately capture the complex nuances of ECG signals.

RQ2. Which are the most adept at accurately encoding the complex representations of ECGs among the SSL methods?

Self-supervised learning (SSL) techniques fundamentally influence the way foundation models represent and process

data. Recent studies suggest that the effectiveness of models trained via generative learning (GL) and contrastive learning (CL) varies depending on their application in specific downstream tasks such as classification and prediction (Dubois et al., 2023). Our research examines how different SSL methods impact the representation of ECG data when tailored to these tasks. We assessed the effectiveness of each model using four distinct metrics: approximation error, representation usability error, probe generalization error, and encoder generalization error, as outlined in the risk decomposition approach (Dubois et al., 2023). Detailed methodologies for these metrics are further elaborated in Section B.1.

RQ3. How can foundation models be effectively implemented within clinical environments to optimize diagnostic processes?

This aspect of our study addresses the deployment of foundation models in scenarios characterized by limited data and scarce labeling resources. We evaluated the performance of the optimal architectural designs identified previously under various conditions of data scarcity. Specifically, we simulated scenarios with case ratio percentages of 1%, 2%, and 5%, and data usage percentages of 10%, 25%, and 50%. The objective is to determine the adaptability and efficacy of these models in diverse real-world situations, assessing their performance across different levels of data availability and their potential reliability and utility in resource-constrained environments.

These questions guide our exploration into the practical applications and theoretical implications of SSL techniques in medical informatics, particularly within the realm of cardiac health diagnostics. The findings from our study are expected to provide valuable insights into the development and deployment of foundation models for ECG analysis, with significant implications for clinical practice and future research directions.

4 Experimental Results

In this section, we provide a summary of the experimental results. Due to paper length limitations, the complete results are included in Appendix C.

4.1 Dataset

For our study, the data was utilized in two primary stages: the foundation model training and the downstream model training and testing.

We used all available unlabeled data for training the foundation model. This extensive use of unlabeled data allowed the foundation model to learn robust and generalized representations of ECG signals through self-supervised learning techniques.

For the downstream tasks, we utilized labeled data. The labeled dataset was split into two parts: 80% of the data was used for training and validation, while the remaining 20% was reserved for the test. It is important to emphasize that the test set was strictly not used during any training step of both the foundation model and the downstream model. This separation ensures that the performance evaluation of the downstream models reflects the foundation models’ ability to generalize to unseen data, thereby providing an unbiased assessment of the foundation models’ effectiveness.

4.2 Environment

The experiments were conducted using a high-performance computing infrastructure equipped with a parallel distributed architecture, including 16 NVIDIA A100 GPUs. This setup facilitated the efficient handling of the extensive datasets and computationally intensive processes required for our study. To ensure consistent training conditions across all phases, we adopted a uniform set of optimization parameters. Throughout the pre-training, linear probing, and fine-tuning stages, we applied a fixed learning rate of 1×10^{-4} and a weight decay of 1×10^{-5} . These parameters were selected to optimize convergence and minimize the risk of overfitting.

The initial stage involved pre-training 81 distinct foundation models (all combinations of 3 patch sizes, 3 block depth, 3 embedding sizes, and 3 SSL methodologies) on a large dataset of 1.1 million unlabeled electrocardiograms (ECGs). This extensive pre-training was conducted over approximately one week for each, aiming to develop robust data representations that form the basis for later supervised learning tasks.

Following SSL pre-training, the top layers of each model were replaced with new linear classifiers, while the underlying base layers retained their pre-trained weights. During this phase, training was restricted to these top layers using a subset of labeled data to assess the effectiveness of the SSL-derived features under the established optimization parameters. This process, known as linear probing, evaluates the quality of the learned representations without updating the pre-trained model’s weights.

After evaluating the models through linear probing, all layers of the models were fine-tuned in a separate phase. This comprehensive fine-tuning phase adapted the entire network’s weights to align more closely with the specific requirements of ECG classification tasks. The consistent application of the predetermined learning rate and weight decay during this stage facilitated a uniform adjustment of the model parameters, enhancing their task-specific performance.

The efficacy of the models was assessed using the Area Under the Receiver Operating Characteristic (AUROC) and the Area Under the Precision-Recall Curve (AUPRC). These metrics provide a robust framework for evaluating the models’ performance across various classification challenges, reflecting their precision and reliability in handling medical data.

4.3 Overall Performance

4.3.1 Foundation Model Loss

Table 3: Variation in losses of foundation models by learning method. Hybrid Learning (HL) achieves lower patient and sample-level losses compared to Contrastive Learning (CL).

	Patch	Depth	Dim	Total loss	Patient loss	Sample loss	Reconstruction loss
CL (Contrastive Learning)	250	2	512	459.2073	262.5800	196.6271	-
GL (Generative Learning)	60	2	1024	11.3272	-	-	11.3272
HL (Hybrid Learning)	60	2	1024	321.2631	135.0332	169.3104	16.9187

The results regarding the loss of foundation models, categorized by the learning methods of Contrastive Learning (CL), Generative Learning (GL), and Hybrid Learning (HL), are summarized in Table 3. Detailed evaluations of the loss variations across different structure settings for these models were extensively analyzed in Appendix C, with the complete results of the evaluation presented in Tables 1, 2, and 3.

The findings illustrated that the structure settings significantly influenced the efficiency of foundation models under different learning frameworks. CL-based models registered the lowest loss with a patch size of 250, suggesting that larger patch sizes enhanced the effectiveness of contrastive mechanisms by encapsulating more comprehensive information cues. Conversely, models based on GL and HL recorded minimal loss at a smaller patch size of 60, indicating a preference for more granular data segmentation in these learning approaches.

Additionally, block depth emerged as a crucial factor affecting model performance, with a depth of 2 blocks proving to be most effective across all models. This highlighted an optimal balance between model complexity and computational manageability. For embedding sizes, CL-based models demonstrated optimal performance with an embedding size of 512, sufficient for capturing essential features without excessive complexity. In contrast, GL and HL models exhibited the best loss metrics at a higher embedding size of 1024, implying a need for more detailed feature extraction to achieve effective learning of ECG representation.

These findings underscored the intricate dependencies between model architectural parameters and their operational efficacy within different SSL paradigms, enriching the understanding of how specific architectural designs could be optimized to enhance the performance of SSL-based foundation models in various applications.

4.3.2 Linear Probing Performance

Table 4: Best performance of linear-probed downstream models and the corresponding structures of foundation model for each SSL method, using Random Init (random initialization of encoder weights) as the baseline.

	Patch	Depth	Dim	AUROC				AUPRC				Criteria
				MI	STTC	CD	HYP	MI	STTC	CD	HYP	
Random Initialization (Baseline)	-	-	-	0.6469	0.7872	0.7261	0.7979	0.4120	0.5844	0.5444	0.3724	4.8713
CL (Contrastive Learning)	250	8	256	0.7849	0.8266	0.7998	0.8467	0.5448	0.5891	0.6019	0.4650	5.4628
GL (Generative Learning)	125	8	512	0.6895	0.8458	0.7520	0.7859	0.4740	0.6442	0.5346	0.4299	5.1559
HL (Hybrid Learning)	125	4	512	0.8318	0.8165	0.8411	0.8135	0.616	0.5911	0.635	0.4140	5.559

Table 4 provided a comprehensive comparison of the linear probing performance with foundation models trained using Contrastive Learning (CL), Generative Learning (GL), and Hybrid Learning (HL) against a baseline model initialized with random encoder weights. The evaluation criteria included AUROC and AUPRC across four downstream tasks: MI, STTC, CD, and HYP.

Performance of the AUROC revealed that the Hybrid Learning (HL) method consistently outperformed the other approaches, achieving the highest AUROC for MI (0.8318) and CD (0.8411). This indicated HL’s superior ability to distinguish between classes in these tasks. Generative Learning (GL) demonstrated the highest AUROC for STTC (0.8458), while Contrastive Learning (CL) led in the HYP task (0.8467). When examining AUPRC, which evaluated the precision-recall trade-off, HL again excelled with the highest AUROC for MI (0.616) and CD (0.635), underscoring its robustness in these predictive tasks. GL, on the other hand, showed the highest AUPRC for STTC (0.6442).

Overall, the performance criteria indicated that Hybrid Learning (HL) achieved the highest score (5.559), suggesting it was the most balanced and effective method among the three evaluated. Contrastive Learning (CL) followed with a score of 5.4628, while Generative Learning (GL) scored 5.1559, both outperforming the baseline of 4.8713. This comprehensive evaluation highlighted the efficacy of Hybrid Learning (HL) in achieving superior performance across various metrics, thereby making it a promising approach for foundation model training in self-supervised learning contexts.

4.3.3 Fine-tuning Performance

Table 5: Best performance of fine-tuned downstream models and the corresponding structures of foundation models for each SSL method, with SL (end-to-end supervised model with labeled data) serving as the baseline.

	Patch	Depth	Dim	AUROC				AUPRC				Criteria
				MI	STTC	CD	HYP	MI	STTC	CD	HYP	
SL (Supervised Learning) (Baseline)	125	2	256	0.9369	0.9380	0.9384	0.9071	0.8571	0.8351	0.8810	0.6769	6.9715
	125	2	512	0.9399	0.9309	0.9397	0.9065	0.8652	0.8101	0.8758	0.6820	6.9501
	125	4	512	0.9404	0.9354	0.9389	0.9167	0.8634	0.8326	0.8780	0.6969	7.0023
CL (Contrastive Learning)	125	2	256	0.9406	0.9426	0.9388	0.9272	0.8686	0.8439	0.8745	0.7086	7.0448
GL (Generative Learning)	125	2	512	0.9389	0.9420	0.9362	0.9191	0.8665	0.8354	0.8753	0.6960	7.0094
HL (Hybrid Learning)	125	4	512	0.9448	0.9398	0.9449	0.9307	0.8809	0.8339	0.8841	0.7153	7.0744

Table 5 illustrates the performance for fine-tuned models based on the various foundation models, with a supervised learning (SL) model serving as the baseline. Among the fine-tuned models, Hybrid Learning (HL) demonstrated the highest AUROC for MI (0.9448) and CD (0.9449), reflecting its superior ability to distinguish between classes in these tasks. Contrastive Learning (CL) achieved the highest AUROC for STTC (0.9426), while also showing strong performance in other tasks. In terms of AUPRC, which evaluates the precision-recall trade-off, HL again excelled with the highest AUPRC for MI (0.8809) and CD (0.8841), further underscoring its robustness in these predictive tasks.

The superior performance of the SSL-based models compared to the SL baseline can be attributed to the inherent advantages of self-supervised learning. SSL-based models leverage vast amounts of unlabeled data to pre-train models, capturing a broad range of patterns and features that might not be as effectively learned through limited labeled data in SL. This extensive pre-training enables foundation models to develop more robust and generalizable representations, which translate to improved performance when fine-tuned on specific downstream tasks. Additionally, SSL approaches like HL and CL facilitate better utilization of the data structure and intrinsic relationships, further enhancing model performance beyond what is achievable with end-to-end supervised learning alone.

Analyzing the task-specific characteristics, each performance of fine-tuned models with the various foundation models reveals insights into their strengths. For Myocardial Infarction (MI) detection, the highest AUROC and AUPRC of fine-tuned model with the HL-based foundation model indicate its effectiveness in identifying subtle variations in heart signals, likely due to its balanced pre-training approach that captures a wide range of features. For ST/T Changes (STTC) detection, the highest AUROC of fine-tuned model with the CL-based foundation model suggests that its contrastive approach, which emphasizes differences between samples, is particularly suited for identifying specific changes in ECG waveforms. In the case of Conduction Disturbance (CD), the highest AUROC and AUPRC of fine-tuned model with the HL-based foundation model highlights its capability to generalize well from pre-training, capturing necessary patterns indicative of conduction disturbances. For Hypertrophy (HYP), detecting structural changes in the heart muscle higher AUROC of fine-tuned model with the CL-based foundation model indicates that contrastive learning is effective in distinguishing features associated with hypertrophy, possibly due to its focus on capturing diverse structural representations.

Overall, the performance criteria suggest that Hybrid Learning (HL) is the most balanced and effective SSL method, achieving the highest overall score. Contrastive Learning (CL) and Generative Learning (GL) also performed well, surpassing the baseline model, but HL’s ability to consistently achieve high scores across multiple tasks highlights its potential as a robust approach for foundation model training in self-supervised learning contexts. The superior

performance of SSL methods across tasks underscores their ability to leverage large-scale unlabeled data for pre-training, capturing complex patterns and relationships that enhance downstream task performance.

4.4 Impact of pre-training strategies on AUROC

To answer the research question, we aim to validate the linear probing and fine-tuning processes on foundation models utilizing different learning methodologies—contrastive learning (CL), generative learning (GL), and a hybrid approach combining both (HL). The four binary classification tasks—Myocardial Infarction (MI), ST/T Changes (STTC), Conduction Disturbance (CD), and Hypertrophy (HYP)—serve as benchmarks to assess the efficacy of these learning techniques under varying parameter settings, such as patch size, embedding size, and block depth.

4.4.1 Patch Size

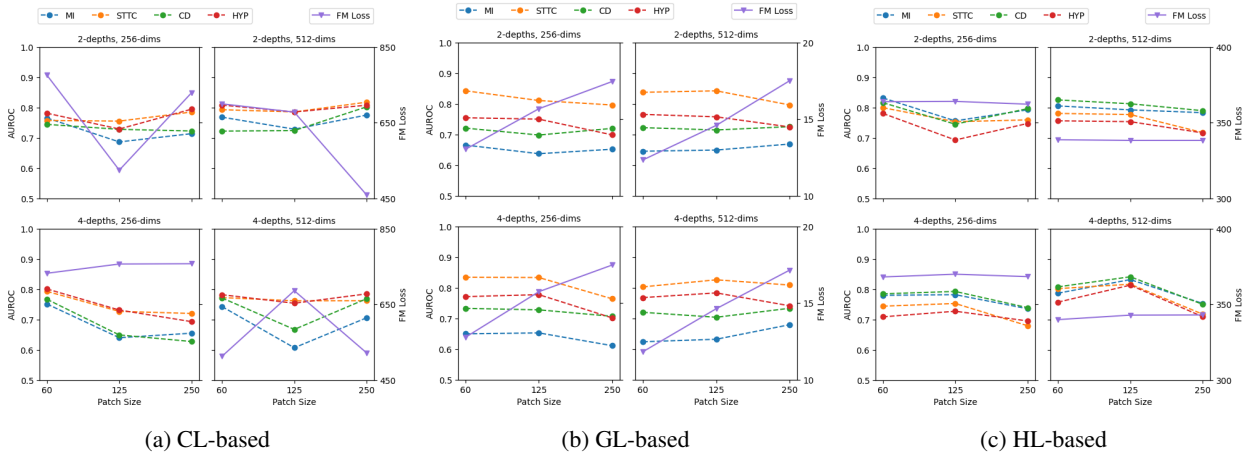


Figure 3: Impact of patch size on the linear probing models

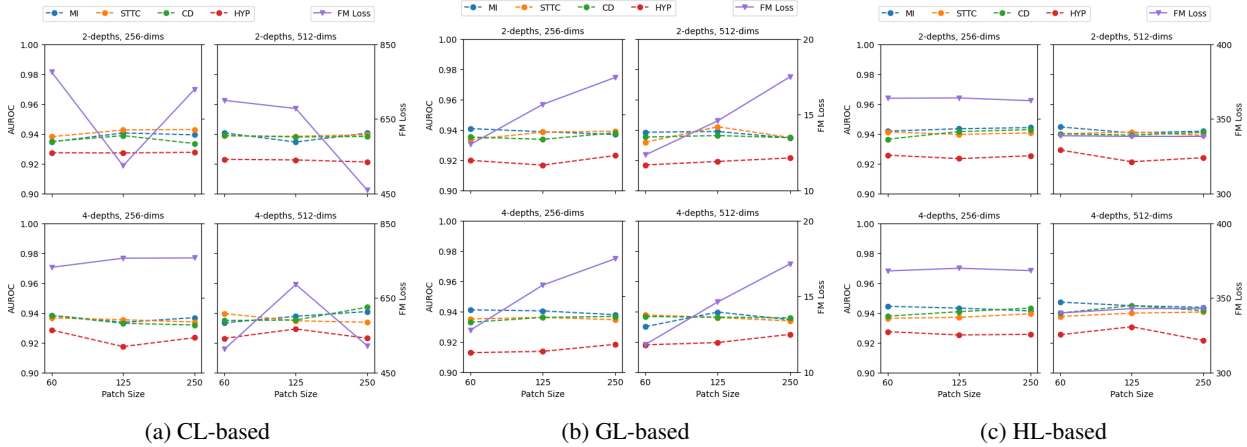


Figure 4: Impact of patch size on the fine-tuning models

Foundation Model Loss: As shown in both Figure 3a and 4a, the loss of CL-based foundation model did not show a consistent trend with patch sizes (e.g., FM Loss showed v-shaped trend with 2-block depth and 256-embedding size, and opposite with 4-block depth and 512-embedding size). The loss of GL-based foundation model showed increasing trend, indicating less learning efficacy in Figure 3b and 4b. In last, the loss of HL-based foundation model also increased with larger patch sizes but less than that of GL-based as depicted in Figure 3c and 4c.

Linear Probing Performance: As shown in Figure 3a, for the linear probing results based on the CL-based foundation model, AUROC for MI generally decreased with larger patch sizes, with a noticeable drop at mid-range patch sizes (e.g., MI AUROC dropped significantly around the 125 patch size). CD and HYP showed slight decreases with larger patch

sizes but were more stable compared to MI, while STTC remained generally stable with slight fluctuations. As shown in Figure 3b, for the linear probing results based on the GL-based foundation model, MI and CD showed improvement with larger patch sizes but with some fluctuations (e.g., AUROC for MI improved from 0.62 to 0.67 as patch size increased with 4-block depth and 512-embedding size), while STTC and HYP showed slight decreases with larger patch sizes. As shown in Figure 3c, for the linear probing results based on the HL-based foundation model demonstrated more stable AUROC for all tasks with slight decreases with larger patch sizes.

Fine-Tuning Performance: In Figure 4a, for the fine-tuning results based on the CL-based foundation model, high and stable AUROC for MI, STTC, CD, and HYP were observed, with slight improvements as patch sizes increased (e.g., MI AUROC remained above 0.93 and slightly improved). As shown in Figure 4b, for the fine-tuning results based on the GL-based foundation model, AUROC remained high and stable across different patch sizes for all tasks, with slight improvements as patch sizes increased (e.g., AUROC for HYP improved on all parameter variations). As depicted in Figure 4c, the HL-based foundation model showed stable AUROC for STTC and CD with slight improvements as patch sizes increased. While the AUROC of MI and HYP were decreased slightly as patch sizes increased. However, the fine-tuning results based on the HL-based foundation model achieved the highest AUROC for MI, STTC, CD, and HYP, further improving with larger patch sizes and FM Loss decreased, indicating effective learning.

4.4.2 Block Depth

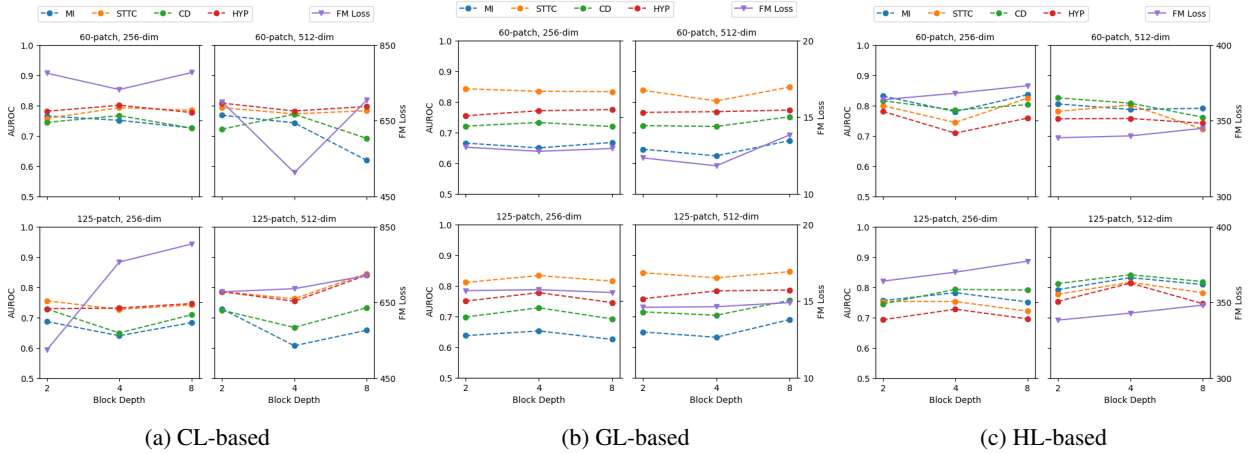


Figure 5: Impact of block depth on the linear probing models

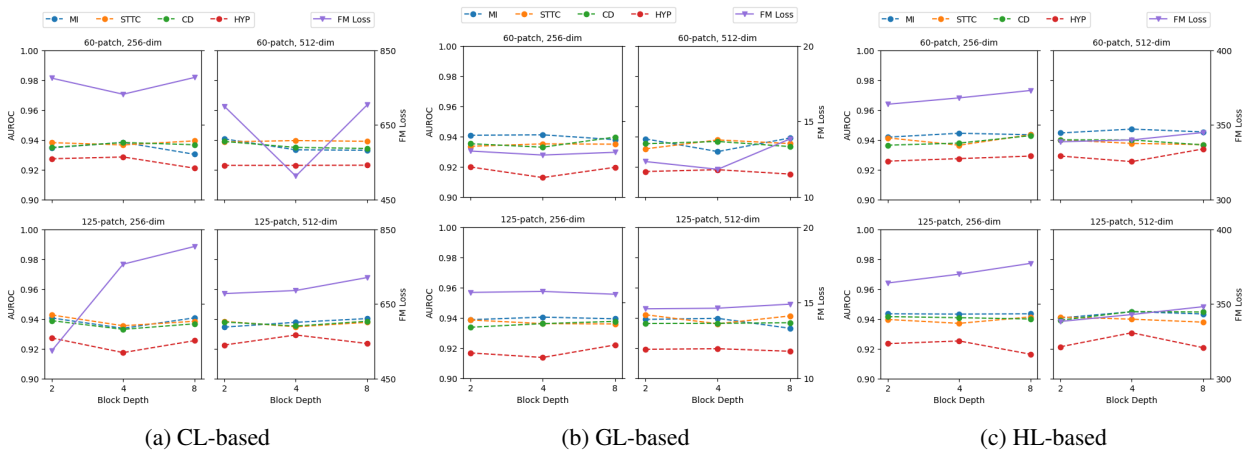


Figure 6: Impact of block depth on the fine-tuning models

Foundation Model Loss: As shown in both Figure 5 and 6, the loss of CL-, GL-, and HL-based foundation model increased with deeper block depth, indicating worse learning (e.g., CL-based FM Loss increased from 524 to 804 with 125-patch size and 256-embedding dims, GL-based FM Loss increased 12.6 to 14.3, and HL-based FM Loss increased from 363 to 368 as block depth increased).

Linear Probing Performance: As shown in Figure 5a, for the linear probing results based on the CL-based foundation model, AUROC for MI, STTC, CD, and HYP generally showed decreases with deeper block depth (e.g., AUROC for CD decreased from 0.72 to 0.69 with deeper block depth). The FM Loss increased with deeper block depth. The linear probing results based on the GL-based foundation model in Figure 5b demonstrated the slight increasing trends, with AUROC showing variability but generally improving with deeper block depth. The linear probing results based on the HL-based foundation model in Figure 5c exhibited better performance compared to other linear probing methods, with AUROC improving slightly with deeper block depth.

Fine-Tuning Performance: For the fine-tuning results based on the CL-based foundation model in Figure 6a, high AUROC for all tasks were observed, slightly improving with deeper block depth (e.g., AUROC for MI increased from 0.93 to 0.94). As shown in Figure 6b, for the fine-tuning results based on the GL-based foundation model, AUROC remained stable across different block depths, with slight improvements. As shown in Figure 6c, the fine-tuning results based on the HL-based foundation model achieved the highest AUROC for all tasks except for HYP, further improving with deeper block depth, while AUROC of HYP slightly decreased with 125-patch size and 256-embedding size.

4.4.3 Embedding Size

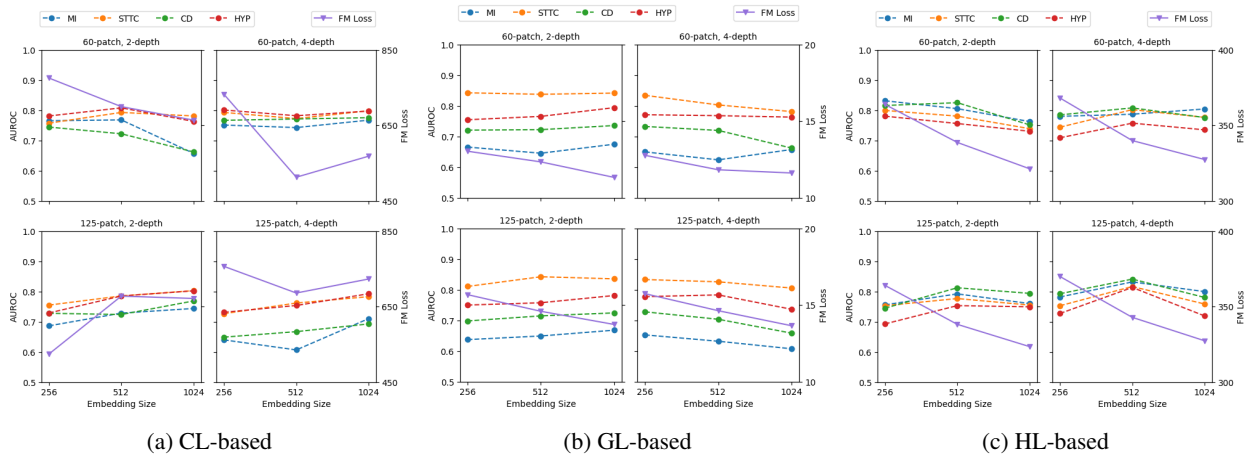


Figure 7: Impact of embedding size on the linear probing models

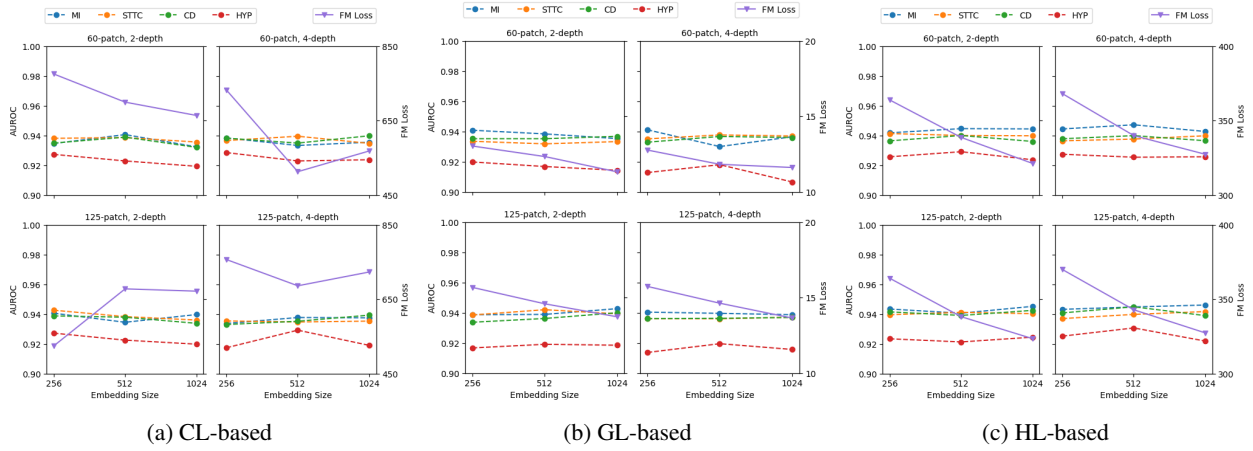


Figure 8: Impact of embedding size on the fine-tuning models

Foundation Model Loss: As depicted in Figure 7 and 8, all FM Loss decreased with larger embedding sizes, indicating better learning (e.g., CL-based FM Loss decreased on all settings except for 125-patch size and 2-block depth, GL-based FM Loss decreased on all settings, and HL-based FM Loss decreased on all settings).

Linear Probing Performance: As shown in Figure 7a, for the linear probing results based on the CL-based foundation model, AUROC for MI, STTC, CD, and HYP generally improved with larger embedding sizes (e.g., AUROC for MI

increased from 0.65 to 0.77 as embedding size increased). The linear probing results based on the GL-based foundation model in Figure 7b demonstrated similar trends in shallow block depth (2-depth), with AUROC improving with larger embeddings but showing slight decreases in deep block depth (4-depth) (e.g., AUROC for all tasks generally improved with larger embeddings with 60-, 125-patch sizes and 2-depth, while decreased with 60-, 125-patch sizes and 4-depth). As shown in Figure 7c, the linear probing results based on the HL-based foundation model showed improvements in AUROC for all tasks with 512 embedding size but slight decreases or consistency with 1,024 embedding sizes.

Fine-Tuning Performance: For the fine-tuning results based on the CL-based foundation model in Figure 8a, AUROC for all tasks were slightly decreased with larger embeddings (e.g., AUROC for HYP decreased in all parameter settings). As shown in Figure 8b, for the fine-tuning results based on the GL-based foundation model, AUROC remained stable across different embedding sizes for all tasks, with slight improvements as embedding sizes increased. The fine-tuning results based on the HL-based foundation model in Figure 8c showed slight improving with larger embedding sizes, further achieving the highest AUROC for all tasks, while FM Loss decreased, indicating effective use of larger embeddings.

4.5 Real-World Applicability

4.5.1 Limited Amount of Data

Table 6: Performance of fine-tuned downstream models based on varying percentages of labeled data usage, excluding 100% data usage detailed in Table 5.

	Data Usage (%)	AUROC				AUPRC				Criteria
		MI	STTC	CD	HYP	MI	STTC	CD	HYP	
SL (Supervised Learning) (Baseline)	50%	0.9311	0.9292	0.9313	0.9049	0.8454	0.8112	0.8623	0.6618	6.8772
	25%	0.9170	0.8991	0.9089	0.8935	0.8184	0.7391	0.8111	0.6446	6.6317
	10%	0.9006	0.9047	0.9017	0.8609	0.7717	0.7545	0.8077	0.6028	6.5046
CL (Contrastive Learning)	50%	0.9361	0.9325	0.9339	0.9212	0.8561	0.8095	0.8583	0.6910	6.9386
	25%	0.9161	0.9249	0.9140	0.9145	0.8235	0.7859	0.8219	0.6817	6.7825
	10%	0.9022	0.9237	0.9064	0.9010	0.8015	0.7828	0.8029	0.6237	6.6442
GL (Generative Learning)	50%	0.9318	0.9338	0.9318	0.9055	0.8586	0.8155	0.8569	0.6689	6.9028
	25%	0.9067	0.9244	0.9236	0.8999	0.8091	0.7906	0.8419	0.6509	6.7471
	10%	0.8885	0.9204	0.8864	0.8883	0.7676	0.7834	0.7774	0.6367	6.5487
HL (Hybrid Learning)	50%	0.9420	0.9332	0.9350	0.9178	0.8760	0.8174	0.8609	0.6968	6.9791
	25%	0.9267	0.9259	0.9268	0.9158	0.8467	0.7882	0.8447	0.7084	6.8832
	10%	0.9182	0.9166	0.9112	0.8655	0.8304	0.7613	0.8064	0.5841	6.5937

Table 6 presents the performance metrics of fine-tuned downstream models based on varying percentages of labeled data usage, excluding 100% data usage. The models evaluated included an end-to-end supervised learning model (SL) and three foundation models pre-trained for each downstream task using Contrastive Learning (CL), Generative Learning (GL), and Hybrid Learning (HL). Performance is measured using AUROC and AUPRC for four downstream tasks (MI, STTC, CD, HYP) and an overall criteria score.

The analysis revealed that as the percentage of labeled data decreased, the performance metrics for all methods dropped. This impact was most significant at 10% data usage, where both AUROC and AUPRC were notably lower. SL demonstrated the steepest decline, indicating its reliance on larger labeled datasets. At 50% data usage, SL showed high AUROC and AUPRC, with a criteria score of 6.8772. However, as data usage dropped to 25% and 10%, its performance decreased, with criteria scores of 6.6317 and 6.5046, respectively.

In contrast, the foundation models exhibited better resilience to reduced labeled data. CL maintained robust performance across all data usage levels, achieving a criteria score of 6.9386 at 50%, 6.7825 at 25%, and 6.6442 at 10%. GL performed comparably to SL at higher data usage levels but showed a slight advantage at lower data usage, with criteria scores of 6.9028 at 50%, 6.7471 at 25%, and 6.5487 at 10%. HL consistently outperformed all other methods, demonstrating the highest AUROC and AUPRC across all tasks. It achieved the highest criteria scores of 6.9791 at 50%, 6.8832 at 25%, and 6.5937 at 10%, indicating superior performance and resilience.

In summary, foundation models, particularly HL, showed superior performance and robustness to reduced labeled data compared to the end-to-end supervised learning model. HL stood out as the most effective approach, maintaining high performance across varying percentages of labeled data usage, followed by CL and GL, while SL showed significant performance degradation with decreased labeled data.

Table 7: Performance of fine-tuned downstream models according to varying case ratios, excluding unchanged case ratios detailed in Table 5.

	Case Ratio (%)	AUROC				AUPRC				Criteria
		MI	STTC	CD	HYP	MI	STTC	CD	HYP	
SL	5%	0.9185	0.9173	0.9168	0.9039	0.8356	0.8001	0.8371	0.6667	6.7960
	2%	0.9045	0.8968	0.8934	0.9115	0.7974	0.7538	0.8017	0.6797	6.6388
	1%	0.8797	0.8969	0.8576	0.8928	0.7684	0.7462	0.7373	0.6281	6.407
CL	5%	0.9234	0.9191	0.9259	0.9208	0.8475	0.7917	0.8441	0.7006	6.8731
	2%	0.9176	0.9167	0.9104	0.9142	0.8237	0.7866	0.8188	0.6747	6.7627
	1%	0.8991	0.9030	0.8921	0.8995	0.7975	0.7442	0.7995	0.6477	6.5826
GL	5%	0.9231	0.9312	0.9247	0.9144	0.8408	0.8132	0.8474	0.6911	6.8859
	2%	0.8912	0.8850	0.9067	0.9052	0.7903	0.7103	0.8169	0.6759	6.5815
	1%	0.8756	0.8856	0.8729	0.8850	0.7536	0.7400	0.7666	0.6389	6.4182
HL	5%	0.9294	0.9278	0.9304	0.9246	0.8636	0.8094	0.8564	0.7080	6.9496
	2%	0.9116	0.9142	0.9113	0.9140	0.8349	0.7759	0.8181	0.6843	6.7643
	1%	0.9069	0.9124	0.9053	0.8816	0.8133	0.7773	0.8175	0.6166	6.6309

4.5.2 Limited Cased of Real-World

Table 7 shows the performance of fine-tuned downstream models that was evaluated according to varying case ratios (5%, 2%, 1%). The models assessed included an end-to-end supervised learning model (SL) and three foundation models pre-trained using Contrastive Learning (CL), Generative Learning (GL), and Hybrid Learning (HL). The fine-tuned models for each downstream task were based on these foundation models. Performance was measured using AUROC (Area Under the Receiver Operating Characteristic Curve) and AUPRC (Area Under the Precision-Recall Curve) for four downstream tasks: MI, STTC, CD, and HYP, with an additional overall criteria score for each model and case ratio.

Across all learning methods, both AUROC and AUPRC metrics generally decreased as the case ratio decreased, indicating a drop in model performance with fewer training cases. However, a key observation is that the Hybrid Learning (HL) model exhibited less performance decline with the drop in case ratio compared to other methods. For instance, in the HL model, the AUROC for MI decreased from 0.9294 at 5% to 0.9069 at 1%, a drop of approximately 2.4%, while the AUPRC for MI fell from 0.8636 to 0.8133, a decline of about 5.8%. This trend indicates that HL models maintain robustness better than CL and GL models under reduced data conditions. For comparison, the AUROC for MI in the CL model decreased from 0.9234 at 5% to 0.8991 at 1%, a drop of around 2.6%, while the AUPRC decreased from 0.8475 to 0.7975, a decline of approximately 5.9%.

Furthermore, the fine-tuned models based on foundation models (CL, GL, and HL) consistently outperformed the end-to-end SL model across all tasks and case ratios. For example, the CL model’s AUROC for MI was 0.9234 at 5% and 0.8991 at 1%, whereas the SL model’s AUROC for MI dropped from 0.9185 at 5% to 0.8797 at 1%, a decrease of about 4.2%. The overall criteria values, reflecting aggregate performance, also decreased with lower case ratios across all learning methods, aligning with the trends observed in AUROC and AUPRC metrics.

Overall, the table demonstrates the robustness and effectiveness of different learning methods under varying data availability conditions, with hybrid learning showing the least performance degradation and fine-tuned models based on foundation models exhibiting superior performance compared to the end-to-end SL model.

4.6 Ablations

4.6.1 Risk decomposition

Table 8 presented a comprehensive risk decomposition analysis (Dubois et al., 2023) across various SSL methodologies—CL, GL, and HL—evaluated over multiple ECG classification tasks (MI, STTC, CD, HYP). Each methodology was assessed across four dimensions of error: approximation, representation usability, probe generalization, and encoder generalization, with a summary of average errors presented in the AVR column.

Approximation Error Our findings revealed significant differences in approximation errors among the methodologies. The CL methodology exhibited the highest approximation errors across nearly all tasks, suggesting that its encoder’s architectural capacity might be insufficient for the complexity of the tasks. This was particularly evident in tasks with higher dimensional data requirements, where the capacity to capture intricate patterns is crucial. In stark contrast, the HL methodology demonstrated robust capabilities by consistently recording the lowest approximation errors, notably excelling in the CD task. This suggests that HL’s architecture is potentially more suited for handling the intricacies of

Table 8: Results of risk decomposition of the fine-tuned downstream models.

	Approximation Error					Representation Usability Error				
	MI	STTC	CD	HYP	AVR.	MI	STTC	CD	HYP	AVR.
CL	0.3600	0.3100	0.3400	0.1300	0.2850	0.0450	0.0200	0.0100	-0.0050	0.0175
GL	0.1300	0.5250	0.3700	0.3850	0.3525	-0.0050	-0.1650	0.0300	-0.0050	-0.0363
HL	0.1000	0.4500	0.3600	0.3500	0.3150	0.0000	-0.1400	-0.0150	0.0300	-0.03125
	Probe Generalization Error					Encoder Generalization Error				
	MI	STTC	CD	HYP	AVR.	MI	STTC	CD	HYP	AVR.
CL	-0.0650	0.0300	-0.0100	-0.0050	-0.0125	0.0700	0.0000	-0.0650	0.0250	0.0075
GL	0.0350	0.2000	-0.0200	-0.0400	0.0438	-0.0200	-0.0600	0.0600	0.1050	0.0213
HL	-0.0600	0.1700	0.0150	0.0200	0.0363	0.0900	0.0200	-0.0600	0.0800	0.0325

ECG data. The GL methodology, while generally performing moderately, showed its best performance in the MI task, indicating a possible alignment of its architectural strengths with the specific demands of this task.

Representation Usability Error Representation usability error analysis further differentiated the methodologies. HL consistently showed the lowest errors, indicating its superior efficacy in generating linearly separable and usable representations for downstream tasks. This is critical in clinical applications where the reliability of ECG classification can directly impact diagnostic outcomes. Conversely, GL’s highest usability error in the MI task suggests its potential limitations in conditions requiring high discriminative power from the representations, which might impede its applicability in more nuanced or complex clinical scenarios.

Probe Generalization Error The probe generalization error results provided insights into the models’ ability to generalize from learned representations to unseen data. The negative values observed in CL’s performance on the STTC task highlight its strengths in generalization, potentially making it suitable for applications where robustness to new data is paramount. However, GL’s relatively high generalization errors, especially in the CD task, underscore some challenges it may face in environments with high variability or where the training data does not comprehensively represent the test scenarios.

Encoder Generalization Error In terms of encoder generalization, HL again proved to be superior, particularly in the STTC and HYP tasks, which suggests that its pretraining approach may better encapsulate the underlying patterns of the ECG data. This robustness is invaluable for practical applications where models often encounter data that differ from the training set. The higher encoder generalization errors observed with the CL methodology indicate potential overfitting to the training data, which could limit its effectiveness in broader clinical implementations.

5 Discussion

5.1 RQ1. What architectural designs of foundation models are most effective for capturing the nuanced semantics of ECG data?

Based on the results from Section 4.4.1, 4.4.2, and 4.4.3, the research question can be answered as follows:

For patch size, our analysis shows that larger patch sizes generally improve performance, especially in fine-tuned configurations. This means that capturing greater contextual information within each patch helps the model better understand broader patterns in the ECG data. For example, in fine tuning, the results of the CL-based foundation model showed high and stable AUROC for all tasks, although there was some improvement as patch size increased. Similarly, the HL-based foundation model achieved the highest AUROC with larger patch sizes. However, in the linear probing results of the GL foundation-based model, the overall performance of all tasks decreased and FM Loss tended to increase. Therefore, for GL-based foundation models, small patch sizes are effective.

In the case of block depth, a slight performance improvement was confirmed in the finetuning results, but these results are not efficient in terms of resource use due to increased model complexity. In addition, linear probing results showed a tendency for performance to decrease and FM loss to increase. These results indicate that the generalizability of the foundation model is reduced. Therefore, it can be said that shallow block depth is efficient for the generalizability of the foundation model and the performance of the downstream model.

For the embedding size, larger embedding sizes consistently improved AUROC across both linear probing and fine-tuning configurations. This indicates that a larger embedding size allows the model to represent more complex features

and patterns within the ECG data. For example, the CL-based method for fine-tuning showed high and stable AUROC, improving with larger embeddings. The HL-based method also achieved the highest AUROC with larger embeddings, indicating that a richer representation space enhances the model’s ability to capture nuanced ECG semantics.

Our analysis shows that the most effective architectural design for a foundation model to capture nuances in ECG data is to use larger patch sizes, shallow block depths, and larger embedding sizes. These design choices allow the base model to capture broader contextual information, represent complex features, and learn hierarchical patterns within ECG data.

5.2 RQ2. Which are the most adept at accurately encoding the complex representations of ECGs among the SSL methods?

Based on the results from Section 4.3.1, 4.3.2, and 4.3.3, the research question can be answered as follows:

Hybrid Learning (HL) emerges as the most adept method at accurately encoding the complex representations of ECGs among the SSL methods evaluated. The table on variation in losses (foundation model losses) showed that HL demonstrated lower patient and sample losses compared to Contrastive Learning (CL). Although HL did not have the lowest total loss, its balanced trade-offs between different loss types suggested its capability to handle complex representations effectively.

In Table 4, HL consistently achieved the highest AUROC and AUPRC in key tasks, particularly for Myocardial Infarction (MI) and Conduction Disturbance (CD). This indicated HL’s superior performance in initial linear probing, showcasing its strength in encoding meaningful ECG representations. Furthermore, in Table 5, HL again outperformed other methods, achieving the highest AUROC for MI and CD, and the highest AUPRC for MI and CD. While Contrastive Learning (CL) excelled in ST/T Changes (STTC), HL’s overall performance was more balanced and robust.

Therefore, HL’s ability to balance various loss types during pre-training, combined with its superior performance in both linear-probed and fine-tuned downstream tasks, highlights its effectiveness in capturing the intricate features and patterns within ECG data. The consistent high performance of HL across multiple evaluation criteria underscores its robustness and reliability in encoding complex ECG representations, making it the most suitable method for this purpose.

5.3 RQ3. How can foundation models be effectively implemented within clinical environments to optimize diagnostic processes?

The analysis of results from Section 4.5 provides insights into effectively implementing foundation models within clinical environments to enhance diagnostic processes.

The study evaluated the performance of optimal architectural designs under conditions of data scarcity by simulating scenarios with case ratio percentages of 1%, 2%, and 5%, and data usage percentages of 10%, 25%, and 50%. These simulations aimed to determine the adaptability and efficacy of the models in diverse real-world situations, assessing their performance across different levels of data availability. The results indicated that Hybrid Learning (HL)-based models maintained robust performance even with limited data, highlighting their potential reliability and utility in resource-constrained environments.

Foundation models, particularly those utilizing HL, have demonstrated significant robustness when dealing with limited labeled data. This adaptability is crucial in clinical environments where obtaining large volumes of annotated medical data is challenging. The ability to perform well with smaller datasets enhances the practicality of these models for clinical use, where data scarcity is a common issue.

Implementing foundation models can enhance diagnostic accuracy. Leveraging pre-trained models fine-tuned with smaller labeled datasets allows healthcare providers to achieve higher diagnostic precision. This is particularly beneficial for detecting conditions with low incidence rates, as the models can be fine-tuned to recognize subtle variations in ECG signals indicative of specific pathologies.

Once pre-trained, foundation models require fewer computational resources for fine-tuning. This efficiency is advantageous for clinical settings where computational resources may be limited. The pre-training phase, involving extensive use of unlabeled data, can be conducted using high-performance computing facilities, while the fine-tuning phase can be performed with more modest computational setups available in clinical environments.

The scalability of foundation models facilitates their application across various clinical tasks beyond ECG analysis. Their flexible architecture can be adapted to other diagnostic processes, such as imaging and genetic data analysis, providing a comprehensive tool for healthcare providers. This versatility is vital for integrating advanced diagnostic models into routine clinical workflows, enhancing overall healthcare delivery.

Incorporating data from diverse sources and demographics during the pre-training phase ensures that foundation models generalize well across different patient populations. This diversity mitigates biases and improves the models' applicability in varied clinical settings, supporting more equitable healthcare outcomes.

Implementing foundation models within clinical environments allows for continuous learning and improvement. Regularly updating the models with new data ensures that diagnostic tools evolve with emerging medical knowledge and patient data trends, maintaining their relevance and accuracy over time.

In conclusion, effectively implementing foundation models within clinical environments involves leveraging their adaptability to limited data, optimizing diagnostic accuracy, ensuring resource efficiency, and maintaining scalability and flexibility. These models provide a robust framework for enhancing diagnostic processes, ultimately contributing to improved patient care and outcomes.

5.4 Comprehensive Analysis

The observed discrepancies in optimal parameter settings across Tables 3, 4, and 5 can be attributed to several factors inherent to the nature of the tasks (loss minimization versus performance maximization) and the characteristics of the different learning methods.

The objectives of these tasks are fundamentally distinct. In Table 3, the goal is to identify parameter settings that minimize total loss, encompassing patient loss, sample loss, and reconstruction loss. This minimization focuses on reducing errors during the pre-training phase, which includes various types of losses depending on the learning method. In contrast, Table 4 aims to maximize the AUROC and AUPRC during linear probing, assessing the quality of pre-trained representations by training a simple classifier on top of the frozen pre-trained model. Table 5 seeks to maximize AUROC and AUPRC during fine-tuning, which involves updating the weights of the entire model, including pre-trained layers, to adapt to specific downstream tasks. The distinct objectives of these tasks naturally lead to different optimal parameter settings.

The nature of the learning methods significantly influences the optimal settings. Contrastive Learning (CL) focuses on learning representations by contrasting positive and negative pairs, implying that the optimal settings for minimizing losses might differ from those providing the best downstream task performance due to the emphasis on distinguishing between similar and dissimilar samples. Generative Learning (GL) focuses on generating data samples that align with the training data distribution. Consequently, the optimal settings for minimizing reconstruction loss may not directly translate to the best settings for discriminative tasks like linear probing and fine-tuning. Hybrid Learning (HL) combines aspects of both contrastive and generative learning, balancing between loss minimization and downstream task performance, which results in different optimal settings for pre-training losses and downstream performance metrics.

The impact of parameter settings also contributes to these differences. Parameters such as patch size, block depth, and embedding size affect the model's capacity and ability to capture different levels of information. Smaller patch sizes capture more detailed information, which is crucial for loss minimization but might not always translate to optimal performance for downstream tasks. For instance, linear probing results based on the CL-based foundation model showed that AUROC for MI generally decreased with larger patch sizes, while CD and HYP exhibited slight decreases and were more stable compared to MI, and STTC remained generally stable with slight fluctuations (Section 4.4.1, Figure 3a). Conversely, larger embedding sizes capture more complex representations, which might benefit linear probing and fine-tuning but could lead to higher pre-training losses if not managed well. The GL-based foundation model demonstrated slight increasing trends, with AUROC generally improving with deeper block depth but showing variability (Section 4.4.2, Figure 5b). Similarly, the HL-based foundation model showed improvements in AUROC for all tasks with a 512 embedding size but exhibited slight decreases or consistency with a 1,024 embedding size (Section 4.4.3, Figure 7c).

Overfitting considerations are crucial in the context of Table 3. Overfitting occurs when a model learns not only the underlying patterns but also the noise in the training data, resulting in poor generalization to new, unseen data. Overfitting risks vary across different parameter settings. In pre-training loss minimization (Table 3), an overemphasis on minimizing total loss could lead to overfitting if the model becomes too tailored to the specific details and noise of the training data. Smaller patch sizes and larger embedding sizes could exacerbate overfitting by capturing more granular details, including noise. To mitigate overfitting, various techniques such as regularization, dropout, and careful monitoring of validation loss can be applied during pre-training.

In conclusion, the differences in optimal parameter settings across the tables arise from the distinct goals and characteristics of the tasks (loss minimization versus performance maximization) and the learning methods (contrastive, generative, hybrid). Each method's nature and the way parameters influence different types of losses and performance metrics lead to varying optimal settings for pre-training and downstream tasks. Overfitting is a crucial factor that needs

to be managed during pre-training to ensure that the models generalize well to new, unseen data. Proper regularization, data augmentation, and careful monitoring of performance metrics are essential to mitigate the risks of overfitting.

5.5 Limitations and Future Works

Limitations Despite the extensive dataset of over 1.1 million ECG samples, the inherent imbalance in medical datasets, particularly in the representation of rare conditions, poses a significant challenge. This imbalance can lead to biased models that perform well on common conditions but poorly on rare ones. Additionally, while the datasets used in this study are comprehensive, they may not fully capture the diversity seen in global populations. Variations in demographic factors such as age, gender, and ethnicity can affect ECG characteristics, and models trained on limited demographic data might not generalize well to all patient populations.

Another critical limitation is model interpretability. Foundation models, especially those based on deep learning architectures like Vision Transformers (ViT), often act as black boxes, making it difficult to interpret their decision-making processes. This lack of transparency can hinder clinical adoption, where understanding the rationale behind a diagnosis is crucial. Furthermore, the pre-training and fine-tuning of large-scale foundation models require significant computational resources, which may not be readily available in all research or clinical settings. This limitation can restrict the accessibility and scalability of these models. Lastly, handling large-scale medical data, particularly ECGs, involves stringent privacy and security considerations. Ensuring that data is anonymized and securely managed is essential, yet challenging, especially when dealing with cross-institutional data sharing.

Future Works To address data imbalance, future work can explore advanced data augmentation techniques and synthetic data generation to create a more balanced and representative dataset, which can help improve model performance on rare conditions. Increasing the diversity of training datasets by including more samples from underrepresented demographic groups can enhance the generalizability of the models. Collaborations with international healthcare institutions could provide access to a more varied patient population.

Developing methods to make the decision-making processes of foundation models more interpretable will be crucial for clinical adoption. Techniques such as attention mechanism visualization, feature importance mapping, and explainable AI (XAI) frameworks can be explored. Research into more efficient training algorithms and model architectures that require less computational power can make these models more accessible. Techniques such as model pruning, quantization, and knowledge distillation can be investigated.

Future work should also focus on developing robust privacy-preserving techniques, such as federated learning and differential privacy, to enable the secure use of sensitive medical data without compromising patient confidentiality. Conducting clinical trials to validate the performance of these foundation models in real-world settings is essential. This will help assess their practical utility and effectiveness in diverse clinical environments. Finally, exploring cross-modal learning techniques that integrate ECG data with other types of medical data (e.g., imaging, genetic information) can provide a more holistic understanding of patient health and improve diagnostic accuracy.

By addressing these limitations and exploring these future directions, the robustness, generalizability, and clinical applicability of foundation models for ECG analysis can be significantly enhanced.

6 Conclusion

This paper presents comprehensive findings on developing and applying foundation models for electrocardiogram (ECG) using Self-Supervised Learning (SSL). The study significantly contributes to the field by pioneering large-scale foundation models specifically tailored for ECG data. These models are trained using a hybrid SSL framework that integrates contrastive and generative learning methods, providing robust and flexible tools for ECG classification in practical healthcare settings. The effectiveness of these models has been demonstrated through extensive testing and optimization processes, focusing on various architectural designs and SSL methods to enhance ECG representation. This involved exploring different parameter architectural designs, which were crucial in determining the optimal settings for achieving the best performance in practical applications, particularly in scenarios with limited labeled data. One of the key conclusions is that while the foundation models excel in ECG classification, the choice of the SSL method significantly impacts their effectiveness. The hybrid learning approach, which combines the strengths of both generative and contrastive learning, has shown superior performance in many cases, suggesting a promising direction for future research and application. Moreover, the study confirms the practical viability of these models in real-world settings, emphasizing the reduced need for labeled data and the potential for quicker, more efficient diagnostic processes. This advancement is expected to facilitate broader adoption and further innovation in the use of deep-learning techniques in cardiology and other medical fields. Ultimately, the findings advocate for continued exploration and development

of foundation models in medical AI, encouraging further studies to refine these models and expand their applications across more varied and complex medical datasets.

References

- J. Devlin, M.-W. Chang, K. Lee, K. Toutanova, Bert: Pre-training of deep bidirectional transformers for language understanding, arXiv preprint arXiv:1810.04805 (2018).
- J. Achiam, S. Adler, S. Agarwal, L. Ahmad, I. Akkaya, F. L. Aleman, D. Almeida, J. Altenschmidt, S. Altman, S. Anadkat, et al., Gpt-4 technical report, arXiv preprint arXiv:2303.08774 (2023).
- T. Chen, S. Kornblith, M. Norouzi, G. Hinton, A simple framework for contrastive learning of visual representations, in: International conference on machine learning, PMLR, 2020, pp. 1597–1607.
- K. He, X. Chen, S. Xie, Y. Li, P. Dollár, R. Girshick, Masked autoencoders are scalable vision learners, in: Proceedings of the IEEE/CVF conference on computer vision and pattern recognition, 2022, pp. 16000–16009.
- A. Baevski, Y. Zhou, A. Mohamed, M. Auli, wav2vec 2.0: A framework for self-supervised learning of speech representations, *Advances in neural information processing systems* 33 (2020) 12449–12460.
- J. Lai, H. Tan, J. Wang, L. Ji, J. Guo, B. Han, Y. Shi, Q. Feng, W. Yang, Practical intelligent diagnostic algorithm for wearable 12-lead ecg via self-supervised learning on large-scale dataset, *Nature Communications* 14 (2023) 3741.
- Y. Wang, Y. Han, H. Wang, X. Zhang, Contrast everything: A hierarchical contrastive framework for medical time-series, *Advances in Neural Information Processing Systems* 36 (2024).
- H.-Y. S. Chien, H. Goh, C. M. Sandino, J. Y. Cheng, Maeeg: Masked auto-encoder for eeg representation learning, arXiv preprint arXiv:2211.02625 (2022).
- Y. Na, M. Park, Y. Tae, S. Joo, Guiding masked representation learning to capture spatio-temporal relationship of electrocardiogram, arXiv preprint arXiv:2402.09450 (2024).
- A. Dosovitskiy, L. Beyer, A. Kolesnikov, D. Weissenborn, X. Zhai, T. Unterthiner, M. Dehghani, M. Minderer, G. Heigold, S. Gelly, et al., An image is worth 16x16 words: Transformers for image recognition at scale, arXiv preprint arXiv:2010.11929 (2020).
- S. Abbaspourzad, O. Elachqar, A. Miller, S. Emrani, U. Nallasamy, I. Shapiro, Large-scale training of foundation models for wearable biosignals, in: The Twelfth International Conference on Learning Representations, 2024.
- Z. Yue, Y. Wang, J. Duan, T. Yang, C. Huang, Y. Tong, B. Xu, Ts2vec: Towards universal representation of time series, in: Proceedings of the AAAI Conference on Artificial Intelligence, volume 36, 2022, pp. 8980–8987.
- Z. Huang, X. Jin, C. Lu, Q. Hou, M.-M. Cheng, D. Fu, X. Shen, J. Feng, Contrastive masked autoencoders are stronger vision learners, *IEEE Transactions on Pattern Analysis and Machine Intelligence* (2023).
- P. Sarkar, A. Etemad, Self-supervised ecg representation learning for emotion recognition, *IEEE Transactions on Affective Computing* 13 (2020) 1541–1554.
- D. Gedon, A. H. Ribeiro, N. Wahlström, T. B. Schön, First steps towards self-supervised pretraining of the 12-lead ecg, *2021 Computing in Cardiology (CinC)* 48 (2021) 1–4.
- H. Liu, Z. Zhao, Q. She, Self-supervised ecg pre-training, *Biomed. Signal Process. Control.* 70 (2021) 103010.
- J. Oh, H. Chung, J. Kwon, D. Hong, E. Choi, Lead-agnostic self-supervised learning for local and global representations of electrocardiogram, *ArXiv abs/2203.06889* (2022).
- A. Atienza, J. Bardram, S. Puthusserypady, Subject-based non-contrastive self-supervised learning for ecg signal processing, *ArXiv abs/2305.10347* (2023).
- Z. Liu, A. Alavi, M. Li, X. Zhang, Self-supervised learning for time series: Contrastive or generative?, arXiv preprint arXiv:2403.09809 (2024).
- A. E. Johnson, T. J. Pollard, L. Shen, L.-w. H. Lehman, M. Feng, M. Ghassemi, B. Moody, P. Szolovits, L. Anthony Celi, R. G. Mark, Mimic-iii, a freely accessible critical care database, *Scientific data* 3 (2016) 1–9.
- A. H. Ribeiro, G. M. Paixao, E. M. Lima, M. Horta Ribeiro, M. M. Pinto Filho, P. R. Gomes, D. M. Oliveira, W. Meira Jr, T. B. Schon, A. L. P. Ribeiro, CODE-15%: a large scale annotated dataset of 12-lead ECGs (2021).
- C. Sudlow, J. Gallacher, N. Allen, V. Beral, P. Burton, J. Danesh, P. Downey, P. Elliott, J. Green, M. Landray, et al., Uk biobank: an open access resource for identifying the causes of a wide range of complex diseases of middle and old age, *PLoS medicine* 12 (2015) e1001779.

- A. L. P. Ribeiro, A. H. Ribeiro, G. M. Paixao, E. M. Lima, M. Horta Ribeiro, M. M. Pinto Filho, P. R. Gomes, D. M. Oliveira, W. Meira Jr, T. B. Schon, E. C. Sabino, Sami-Trop: 12-lead ECG traces with age and mortality annotations (2021).
- M. Seják, J. Sido, D. Žahour, Ikem dataset v1.0.0 (2023).
- S. Woo, S. Debnath, R. Hu, X. Chen, Z. Liu, I. S. Kweon, S. Xie, Convnext v2: Co-designing and scaling convnets with masked autoencoders, in: Proceedings of the IEEE/CVF Conference on Computer Vision and Pattern Recognition, 2023, pp. 16133–16142.
- Y. Dubois, T. Hashimoto, P. Liang, Evaluating self-supervised learning via risk decomposition, arXiv preprint arXiv:2302.03068 (2023).

A Data sets

A.1 Summary of Data sets

This section provides a detailed description of the various datasets used in the study, including MIMIC-IV, CODE15, UK Biobank, SaMi-Trop, and IKEM. Each dataset description includes demographic information, the number of samples, and specific details about the data collection and characteristics.

MIMIC-IV (Johnson et al., 2016) is an extensive database that contains comprehensive data on patients admitted to a tertiary academic medical center in Boston, MA, USA. The database provides a wealth of information about each patient while hospitalized, including laboratory measurements, medications administered, documented vital signs, and other relevant medical data. The primary aim of this database is to support healthcare research.

CODE15 (Ribeiro et al., 2021) is a dataset of 345,779 ECG exams from 233,770 patients. The ECGs were sampled at a rate of 400 Hz and had varying durations, but were standardized to ECGs of 4096 points by filling them with zeros on both sides.

UK Biobank (Sudlow et al., 2015) is a publicly available dataset containing data on 500,000 individuals from the United Kingdom. This population-based study includes individuals aged 40 to 69 years old who were recruited between 2006 and 2010. Resting 12-lead ECGs and interval measurements were available for 15,365 participants, and 13,314 were included in the analysis after excluding those with AF on ECG or AF identified from self-reports at baseline or electronic healthcare records.

SaMi-Trop (Ribeiro et al., 2021) is a prospective cohort study funded by the NIH. It includes 1,959 patients with chronic Chagas cardiomyopathy and aims to evaluate the usefulness of a clinical prediction rule based on ECG, brain natriuretic peptide (BNP) levels, and other biomarkers in clinical practice. A subset of the SaMi-Trop dataset with annotations of age and mortality and the correspondent ECG traces is openly available.

IKEM (Sejak et al., 2023) is a dataset of 12-lead ECG recordings collected from patients examined by the cardiology or diabetology sections at the Institute for Clinical and Experimental Medicine (IKEM) in Prague, Czech Republic. The recordings were sampled at a rate of 500 Hz for 10 seconds each. Each entry in the dataset includes raw ECG recordings paired with an anonymized unique patient ID, which groups ECG recordings belonging to the same patient.

A.2 Characteristics of ECG Annotations

This section elaborates on the annotated classes used in the study, including Myocardial Infarction (MI), ST/T Changes (STTC), Conduction Disturbance (CD), and Hypertrophy (HYP). It includes descriptions of each condition, their significance, and the typical ECG characteristics associated with each.

MI (Myocardial Infarction)

- **Description:** Myocardial Infarction, commonly known as a heart attack, involves the interruption of blood supply to a part of the heart, causing heart cells to die. This is typically caused by a blockage in one or more coronary arteries due to plaque (a mix of fat, cholesterol, and other substances).
- **ECG Characteristics:** The ECG of a person suffering from MI may show abnormal Q waves, elevation or depression of the ST segment, and T wave inversions. Diagnosing MI involves identifying these specific patterns on different parts of the ECG.

STTC (ST/T Changes)

- **Description:** ST/T changes on an ECG can indicate various conditions including cardiac ischemia, electrolyte imbalances, and other myocardial injuries. The ST segment and T wave are parts of the ECG cycle associated with the heart’s electrical recovery (repolarization) following a contraction.
- **ECG Characteristics:** ST segment elevations can indicate acute myocardial injury (like in the case of an ongoing heart attack), while ST depressions and T wave inversions can suggest coronary ischemia or other cardiac problems.

CD (Conduction Disturbance)

- **Description:** Conduction disturbances occur when the heart’s electrical impulses are delayed or blocked at certain points in the heart’s conduction system (such as the AV node or the His-Purkinje system). This can lead to arrhythmias or irregular heartbeats.

- **ECG Characteristics:** ECG patterns may include prolonged PR intervals, widened QRS complexes, or abnormal QRS morphologies depending on where the blockage occurs. Conditions such as Bundle Branch Blocks or AV blocks are examples.

HYP (Hypertrophy)

- **Description:** Hypertrophy in the cardiac context usually refers to the thickening of the heart muscle, typically the left ventricle, which can be caused by chronic high blood pressure or other diseases that increase the workload of the heart.
- **ECG Characteristics:** ECG signs of hypertrophy involve larger than the normal voltage in QRS complexes, changes in the ST segment and T wave and a shift in the axis of the QRS wave. These changes reflect the increased muscle mass and altered electrical conduction due to the thickening walls.

Each of these tasks requires the AI model to recognize specific and often subtle variations in ECG waveforms to accurately classify the type of cardiac event or condition. The performance of these tasks in AI models, as measured by AUROC, indicates how well these patterns can be detected and classified against a backdrop of normal and other abnormal patterns.

B Evaluation Metrics

B.1 AUROC and AUPRC Calculations

An explanation of the evaluation metrics used in the study, including the calculation of Area Under the Receiver Operating Characteristic (AUROC) and Area Under the Precision-Recall Curve (AUPRC). This section provides the formulas and interpretation guidelines for these metrics.

- **AUROC:** The Area Under the Receiver Operating Characteristic (AUROC) curve is a statistical measure that evaluates the performance of binary classification models. AUROC plots the True Positive Rate (TPR) versus the False Positive Rate (FPR) at different threshold settings. It represents the probability of a classifier ranking a randomly chosen positive instance higher than a randomly chosen negative one. An AUC of 1 indicates perfect classification, while an AUC of 0.5 suggests performance equivalent to random guessing. AUROC is useful for evaluating models on imbalanced datasets as it is not influenced by class label distribution.
- **AUPRC:** The Area Under the Precision-Recall Curve (AUPRC) provides a measure to evaluate binary classification model performance, especially under class imbalance. Unlike AUROC, which plots TPR against FPR, PRC plots Precision (true positives to all predicted positives) against Recall (equivalent to TPR). A higher AUPRC value represents better performance in distinguishing between classes under imbalanced class distributions.
- **F1-Score:** The F1-Score, a harmonic mean of Precision and Recall, offers a balance between the two metrics for binary classification models. It is calculated as $2 * (Precision * Recall) / (Precision + Recall)$, where Precision is the ratio of true positives to the sum of true and false positives, and Recall is the ratio of true positives to the sum of true positives and false negatives. The F1-Score ranges from 0 to 1, where 1 indicates perfect Precision and Recall, and 0 indicates the worst. The F1-Score is particularly useful when the costs of false positives and false negatives are similar, and when class distribution is imbalanced.

B.2 Risk Decomposition

Details on the risk decomposition approach (Dubois et al., 2023) used to evaluate the self-supervised learning methods. It includes descriptions of approximation error, representation usability error, probe generalization error, and encoder generalization error, along with how these were measured and analyzed.

- **Encoder generalization error:** The encoder generalization error measures the drop in performance due to pretraining the encoder on finite samples U compared to the population p_{un} . Intuitively, it is small if: (i) A_ϕ makes the pre-training sample efficient, or (ii) there are many pre-training examples $|U|$.
- **Probe generalization error:** The probe generalization error measures the drop in performance due to training the probe on finite samples S instead of p_{sup} . Intuitively, it is small if: (i) the number of training samples $|S|$ is large, or (ii) representations ensure that downstream probes are sample efficient, e.g., by minimizing the margin between same-class examples.

- **Representation usability error:** The representation usability error measures errors due to learning representations via an SSL pipeline A_ϕ, p_{un} , rather than supervised learning. Intuitively, it is small if the SSL algorithm ensures that representations retain information usable by probes F , e.g., linearly separable classes.
- **Approximation error:** The approximation error measures errors due to the architecture of the encoder ϕ (e.g., ResNet50) and probes F (e.g., linear) being too constrained to perform even the supervised task. Intuitively, it decreases with the capacity of ϕ, F .

C Experimental Results

This section provides an entire experimental results. The initial stage involved pre-training 81 distinct foundation models (all combinations of 3 patch sizes, 3 block depth, 3 embedding sizes, and 3 SSL methodologies) on a large dataset of 1.1 million unlabeled electrocardiograms (ECGs). Following SSL pre-training, the top layers of each model were replaced with new linear classifiers, while the underlying base layers retained their pre-trained weights. After evaluating the models through linear probing, all layers of the models were fine-tuned in a separate phase.

C.1 Pre-training Results

Detailed tables showing the losses of different foundation model architectures (e.g., patch size, block depth, embedding size) in pre-training, demonstrating how each parameter affects to pre-train.

Table 1: The result of CL-based foundation models.

Case	Windows	Depth	Dims	Total loss	Patient loss	Sample loss	Reconstruction loss
0	60	2	256	775.3041	441.5192	333.7850	N/A
1	60	2	512	699.6405	414.7109	284.9303	N/A
2	60	2	1024	663.8318	544.7585	119.0735	N/A
3	60	4	256	732.1746	418.5121	313.6624	N/A
4	60	4	512	512.7451	291.5426	221.2027	N/A
5	60	4	1024	568.3319	326.3327	241.9992	N/A
6	60	8	256	777.0902	439.2020	337.8884	N/A
7	60	8	512	703.6331	553.8072	149.8258	N/A
8	60	8	1024			OOM	
9	125	2	256	524.5357	284.3040	240.2327	N/A
10	125	2	512	677.8004	397.1795	280.6209	N/A
11	125	2	1024	671.6511	399.2603	272.3903	N/A
12	125	4	256	756.5930	426.3842	330.2094	N/A
13	125	4	512	686.0510	511.8934	174.1582	N/A
14	125	4	1024	723.0967	428.0925	295.0038	N/A
15	125	8	256	804.1048	449.9247	354.1809	N/A
16	125	8	512	720.7618	546.3441	174.4180	N/A
17	125	8	1024			OOM	
18	250	2	256	729.0459	418.5083	310.5373	N/A
19	250	2	512	459.2073	262.5800	196.6271	N/A
20	250	2	1024	727.0769	455.8883	271.1887	N/A
21	250	4	256	757.3063	439.1334	318.1726	N/A
22	250	4	512	521.8998	297.6395	224.2606	N/A
23	250	4	1024	673.0448	521.9521	151.0925	N/A
24	250	8	256	767.0340	432.2636	334.7702	N/A
25	250	8	512	724.7963	420.9260	303.8701	N/A
26	250	8	1024			OOM	

C.2 Linear Probing Results

Detailed tables showing the performance of different foundation model architectures (e.g., patch size, block depth, embedding size) in linear probing. This section should include AUROC and AUPRC for various settings, demonstrating how each parameter affects model performance.

C.3 Fine-tuning Results

Detailed tables showing the performance of different foundation model architectures (e.g., patch size, block depth, embedding size) in fine-tuning. It provides a comprehensive comparison of AUROC and AUPRC across different foundation model configurations and self-supervised learning methods.

Table 2: The result of GL-based foundation models.

Case	Windows	Depth	Dims	Total loss	Patient loss	Sample loss	Reconstruction loss
0	60	2	256	13.0357	N/A	N/A	13.0357
1	60	2	512	12.3399	N/A	N/A	12.3399
2	60	2	1024	11.3272	N/A	N/A	11.3272
3	60	4	256	12.7696	N/A	N/A	12.7696
4	60	4	512	11.8257	N/A	N/A	11.8257
5	60	4	1024	11.6158	N/A	N/A	11.6158
6	60	8	256	12.9540	N/A	N/A	12.9540
7	60	8	512	13.8394	N/A	N/A	13.8394
8	60	8	1024	11.3917	N/A	N/A	11.3917
9	125	2	256	15.6771	N/A	N/A	15.6771
10	125	2	512	14.5915	N/A	N/A	14.5915
11	125	2	1024	13.7325	N/A	N/A	13.7325
12	125	4	256	15.7419	N/A	N/A	15.7419
13	125	4	512	14.6308	N/A	N/A	14.6308
14	125	4	1024	13.6501	N/A	N/A	13.6501
15	125	8	256	15.5542	N/A	N/A	15.5542
16	125	8	512	14.8993	N/A	N/A	14.8993
17	125	8	1024	13.1519	N/A	N/A	13.1519
18	250	2	256	17.4541	N/A	N/A	17.4541
19	250	2	512	17.5024	N/A	N/A	17.5024
20	250	2	1024	17.1858	N/A	N/A	17.1858
21	250	4	256	17.4811	N/A	N/A	17.4811
22	250	4	512	17.1457	N/A	N/A	17.1457
23	250	4	1024	16.9634	N/A	N/A	16.9634
24	250	8	256	17.5896	N/A	N/A	17.5896
25	250	8	512	17.3625	N/A	N/A	17.3625
26	250	8	1024	17.1834	N/A	N/A	17.1834

Table 3: The results of HL-based foundation models.

Case	Windows	Depth	Dims	Total loss	Patient loss	Sample loss	Reconstruction loss
0	60	2	256	363.8454	153.4615	191.6084	18.7758
1	60	2	512	338.7160	143.0586	176.5117	19.1446
2	60	2	1024	321.2631	135.0332	169.3104	16.9187
3	60	4	256	368.1020	157.6347	191.3426	19.1249
4	60	4	512	339.9288	143.6038	178.7828	17.5419
5	60	4	1024	327.3949	139.2565	170.1599	17.9787
6	60	8	256	373.0694	158.4789	195.4308	19.1591
7	60	8	512	344.9142	147.0694	179.0293	18.8156
8	60	8	1024			OOM	
9	125	2	256	364.0501	149.6521	194.6952	19.7029
10	125	2	512	338.2749	138.8596	180.2473	19.1674
11	125	2	1024	323.5201	134.1882	170.3779	18.9548
12	125	4	256	369.9288	153.7398	196.6635	19.5256
13	125	4	512	342.8939	142.0322	181.1545	19.7073
14	125	4	1024	327.3968	138.0119	169.6444	19.7404
15	125	8	256	377.1915	158.0082	199.4338	19.7494
16	125	8	512	348.1791	146.8680	181.5616	19.7499
17	125	8	1024			OOM	
18	250	2	256	362.1963	148.8520	193.6936	19.6514
19	250	2	512	338.2755	137.9361	180.6892	19.6513
20	250	2	1024	324.4859	131.7396	173.0957	19.6511
21	250	4	256	368.3145	151.1946	197.4695	19.6514
22	250	4	512	343.0133	140.4411	182.9213	19.6512
23	250	4	1024	328.0620	138.0024	170.4090	19.6509
24	250	8	256			OOM	
25	250	8	512			OOM	
26	250	8	1024			OOM	

Table 4: The linear probing results of CL-based foundation models.

Case	Windows	Depth	Dims	AUROC				AUPRC				Criteria
				MI	STTC	CD	HYP	MI	STTC	CD	HYP	
0	60	2	256	0.7653	0.7573	0.7443	0.7811	0.5147	0.4614	0.4073	0.2922	4.7236
1	60	2	512	0.7681	0.7928	0.7221	0.808	0.5421	0.5265	0.4909	0.3533	5.0038
2	60	2	1024	0.6574	0.7811	0.6621	0.7631	0.406	0.4776	0.3591	0.3008	4.4072
3	60	4	256	0.7511	0.7928	0.7667	0.8008	0.531	0.5268	0.5469	0.3331	5.0492
4	60	4	512	0.7427	0.7724	0.7712	0.7819	0.5341	0.5019	0.4991	0.309	4.9123
5	60	4	1024	0.7673	0.7984	0.7754	0.7974	0.5418	0.533	0.4994	0.341	5.0537
6	60	8	256	0.726	0.7844	0.7253	0.7769	0.4692	0.4961	0.4311	0.3017	4.7107
7	60	8	512	0.619	0.7829	0.6916	0.7967	0.3647	0.4956	0.427	0.339	4.5165
8	60	8	1024					OOM				
9	125	2	256	0.6864	0.7551	0.7279	0.729	0.3884	0.4815	0.4208	0.2498	4.4389
10	125	2	512	0.7285	0.7854	0.7239	0.7852	0.4609	0.4844	0.396	0.3033	4.6676
11	125	2	1024	0.7439	0.8029	0.7688	0.8024	0.483	0.5247	0.4732	0.336	4.9349
12	125	4	256	0.6399	0.7268	0.649	0.7313	0.3611	0.416	0.3065	0.2475	4.0781
13	125	4	512	0.6067	0.7618	0.6672	0.7537	0.3293	0.4993	0.3689	0.2952	4.2821
14	125	4	1024	0.7102	0.783	0.6927	0.7926	0.4333	0.4958	0.3641	0.3221	4.5938
15	125	8	256	0.6832	0.7414	0.7091	0.7461	0.4236	0.4705	0.3826	0.2563	4.4128
16	125	8	512	0.6579	0.8453	0.7323	0.8399	0.4166	0.6127	0.4673	0.4371	5.0091
17	125	8	1024					OOM				
18	250	2	256	0.7137	0.7851	0.7225	0.7945	0.4471	0.5159	0.4073	0.3621	4.7482
19	250	2	512	0.775	0.8177	0.8022	0.8077	0.5637	0.5982	0.5872	0.411	5.3627
20	250	2	1024	0.7283	0.8045	0.7382	0.8138	0.4571	0.5481	0.4335	0.3632	4.8867
21	250	4	256	0.6548	0.72	0.6273	0.6929	0.3687	0.432	0.2859	0.2178	3.9994
22	250	4	512	0.7056	0.762	0.7687	0.7846	0.4464	0.5035	0.5168	0.3299	4.8175
23	250	4	1024	0.7179	0.8048	0.7601	0.7971	0.489	0.5645	0.5163	0.3213	4.971
24	250	8	256	0.7849	0.8266	0.7998	0.8467	0.5488	0.5891	0.6019	0.465	5.4628
25	250	8	512	0.7383	0.8027	0.7844	0.8047	0.5081	0.5307	0.5225	0.3821	5.0735
26	250	8	1024					OOM				

Table 5: The linear probing results of GL-based foundation models.

Case	Windows	Depth	Dims	AUROC				AUPRC				Criteria
				MI	STTC	CD	HYP	MI	STTC	CD	HYP	
0	60	2	256	0.6653	0.8424	0.7206	0.7545	0.46	0.6523	0.4777	0.3484	4.9212
1	60	2	512	0.6453	0.8375	0.7222	0.7655	0.4394	0.6571	0.4802	0.3689	4.9161
2	60	2	1024	0.6747	0.8415	0.7356	0.794	0.4748	0.6545	0.5087	0.4247	5.1085
3	60	4	256	0.6496	0.8342	0.7326	0.7709	0.4558	0.6376	0.4815	0.3877	4.9499
4	60	4	512	0.6237	0.8028	0.7197	0.7678	0.4054	0.6039	0.4751	0.3787	4.7771
5	60	4	1024	0.6574	0.7811	0.6621	0.7631	0.406	0.4776	0.3591	0.3008	4.4072
6	60	8	256	0.6674	0.8331	0.7191	0.7747	0.4685	0.644	0.469	0.4217	4.9975
7	60	8	512	0.6734	0.848	0.751	0.7731	0.4797	0.643	0.5452	0.4061	5.1195
8	60	8	1024	0.6418	0.8267	0.7404	0.7936	0.4336	0.6211	0.542	0.4029	5.0021
9	125	2	256	0.6372	0.8107	0.6981	0.7499	0.4241	0.6086	0.4531	0.3777	4.7594
10	125	2	512	0.6491	0.8423	0.7147	0.7575	0.439	0.6539	0.463	0.3695	4.889
11	125	2	1024	0.668	0.8355	0.7244	0.7811	0.4586	0.6401	0.4721	0.4191	4.9989
12	125	4	256	0.6526	0.8332	0.7278	0.7774	0.4395	0.6502	0.5002	0.41	4.9909
13	125	4	512	0.6319	0.8258	0.7036	0.7831	0.4237	0.6275	0.4505	0.4093	4.8554
14	125	4	1024	0.6073	0.8054	0.6583	0.7362	0.4028	0.6002	0.4081	0.3282	4.5465
15	125	8	256	0.625	0.8148	0.6917	0.745	0.4269	0.6121	0.4701	0.3674	4.753
16	125	8	512	0.6895	0.8458	0.752	0.7859	0.474	0.6442	0.5346	0.4299	5.1559
17	125	8	1024	0.6627	0.8294	0.7521	0.7745	0.4688	0.6112	0.5514	0.3924	5.0425
18	250	2	256	0.6518	0.7961	0.7198	0.6986	0.4272	0.5703	0.4891	0.3168	4.6697
19	250	2	512	0.6687	0.7963	0.7254	0.7245	0.4445	0.5769	0.5001	0.3333	4.7697
20	250	2	1024	0.6733	0.8091	0.7306	0.7475	0.4564	0.5872	0.5067	0.3594	4.8702
21	250	4	256	0.6109	0.7638	0.7067	0.7015	0.351	0.5324	0.4738	0.3006	4.4407
22	250	4	512	0.6793	0.8087	0.7329	0.7411	0.4496	0.5843	0.5165	0.3744	4.8868
23	250	4	1024	0.6758	0.8109	0.7104	0.751	0.4497	0.5968	0.4664	0.3725	4.8335
24	250	8	256	0.5489	0.7022	0.6514	0.6327	0.3123	0.4832	0.4112	0.259	4.0009
25	250	8	512	0.6544	0.7945	0.7151	0.7283	0.4294	0.5793	0.4957	0.3478	4.7445
26	250	8	1024	0.6412	0.77	0.6817	0.7473	0.406	0.5298	0.4278	0.34	4.5438

Table 6: The linear probing results of HL-based foundation models.

Case	Windows	Depth	Dims	AUROC				AUPRC				Criteria
				MI	STTC	CD	HYP	MI	STTC	CD	HYP	
0	60	2	256	0.8314	0.7994	0.8158	0.7804	0.658	0.5861	0.6086	0.3635	5.4432
1	60	2	512	0.8053	0.7805	0.8251	0.7561	0.5942	0.5281	0.6074	0.308	5.2047
2	60	2	1024	0.7626	0.7391	0.7516	0.7305	0.5408	0.4679	0.4719	0.2982	4.7626
3	60	4	256	0.7799	0.744	0.7848	0.7089	0.5488	0.4986	0.5261	0.2702	4.8613
4	60	4	512	0.7869	0.802	0.8078	0.7573	0.5702	0.5417	0.5553	0.3002	5.1214
5	60	4	1024	0.8042	0.7765	0.7759	0.7352	0.5843	0.4947	0.5051	0.2522	4.9281
6	60	8	256	0.8357	0.8245	0.803	0.7585	0.6575	0.5799	0.5782	0.3395	5.3768
7	60	8	512	0.7908	0.7225	0.7616	0.7414	0.5368	0.439	0.4635	0.2875	4.7431
8	60	8	1024					OOM				
9	125	2	256	0.7559	0.7531	0.7449	0.6928	0.5257	0.4739	0.4317	0.225	4.603
10	125	2	512	0.7922	0.7768	0.8124	0.7533	0.5701	0.5317	0.573	0.2996	5.1091
11	125	2	1024	0.7601	0.7552	0.7939	0.7494	0.5311	0.4868	0.5193	0.2978	4.8936
12	125	4	256	0.782	0.7529	0.7927	0.7273	0.5664	0.4789	0.506	0.2593	4.8655
13	125	4	512	0.8318	0.8165	0.8411	0.8135	0.616	0.5911	0.635	0.414	5.559
14	125	4	1024	0.7997	0.7587	0.7804	0.7192	0.556	0.4941	0.5006	0.2733	4.882
15	125	8	256	0.7514	0.7209	0.7905	0.6954	0.5087	0.4441	0.5068	0.2722	4.69
16	125	8	512	0.8088	0.7817	0.8187	0.7457	0.6041	0.5396	0.5897	0.3041	5.1924
17	125	8	1024					OOM				
18	250	2	256	0.7925	0.7592	0.7964	0.7473	0.5825	0.4862	0.5088	0.2928	4.9657
19	250	2	512	0.783	0.7173	0.7896	0.7162	0.5506	0.4566	0.5378	0.2515	4.8026
20	250	2	1024	0.818	0.8061	0.8155	0.7702	0.597	0.5615	0.593	0.3473	5.3086
21	250	4	256	0.7356	0.6794	0.7391	0.6953	0.4949	0.3881	0.4304	0.2596	4.4224
22	250	4	512	0.7531	0.7177	0.7501	0.7093	0.5213	0.4241	0.4643	0.236	4.5759
23	250	4	1024	0.7815	0.7504	0.8015	0.7608	0.5264	0.459	0.5574	0.3165	4.9535
24	250	8	256					OOM				
25	250	8	512					OOM				
26	250	8	1024					OOM				

Table 7: The fine-tuning results of CL-based foundation models.

Case	Windows	Depth	Dims	AUROC				AUPRC				Criteria
				MI	STTC	CD	HYP	MI	STTC	CD	HYP	
0	60	2	256	0.9346	0.9381	0.9349	0.9273	0.8580	0.8263	0.8771	0.7015	6.9978
1	60	2	512	0.9406	0.9386	0.9389	0.9229	0.8647	0.8176	0.8752	0.6947	6.9932
2	60	2	1024	0.9324	0.9356	0.9320	0.9193	0.8549	0.8240	0.8636	0.6846	6.9464
3	60	4	256	0.9383	0.9366	0.9382	0.9285	0.8610	0.8215	0.8786	0.7011	7.0038
4	60	4	512	0.9333	0.9395	0.9349	0.9229	0.8456	0.8326	0.8654	0.6898	6.9640
5	60	4	1024	0.9355	0.9347	0.9398	0.9237	0.8589	0.8168	0.8770	0.6749	6.9613
6	60	8	256	0.9303	0.9393	0.9367	0.9210	0.8570	0.8304	0.8712	0.6883	6.9742
7	60	8	512	0.9330	0.9390	0.9342	0.9230	0.8586	0.8319	0.8709	0.6981	6.9887
8	60	8	1024					OOM				
9	125	2	256	0.9406	0.9426	0.9388	0.9272	0.8686	0.8439	0.8745	0.7086	7.0448
10	125	2	512	0.9345	0.9383	0.9379	0.9225	0.8527	0.8258	0.8813	0.6954	6.9884
11	125	2	1024	0.9397	0.9360	0.9338	0.9198	0.8668	0.8209	0.8729	0.6886	6.9785
12	125	4	256	0.9337	0.9354	0.9330	0.9174	0.8574	0.8199	0.8730	0.6675	6.9373
13	125	4	512	0.9377	0.9347	0.9352	0.9292	0.8634	0.8291	0.8711	0.7085	7.0089
14	125	4	1024	0.9375	0.9353	0.9393	0.9190	0.8638	0.8282	0.8806	0.6940	6.9977
15	125	8	256	0.9407	0.9384	0.9367	0.9254	0.8702	0.8255	0.8764	0.6972	7.0105
16	125	8	512	0.9402	0.9377	0.9384	0.9235	0.8651	0.8266	0.8747	0.6888	6.9950
17	125	8	1024					OOM				
18	250	2	256	0.9393	0.9429	0.9335	0.9276	0.8699	0.8410	0.8694	0.6984	7.0220
19	250	2	512	0.9405	0.9394	0.9382	0.9211	0.8687	0.8373	0.8730	0.7014	7.0196
20	250	2	1024	0.9366	0.9396	0.9318	0.9232	0.8625	0.8318	0.8661	0.6960	6.9876
21	250	4	256	0.9368	0.9339	0.9319	0.9234	0.8670	0.8158	0.8724	0.7022	6.9834
22	250	4	512	0.9409	0.9337	0.9438	0.9230	0.8679	0.8354	0.8825	0.7024	7.0296
23	250	4	1024	0.9349	0.9369	0.9333	0.9249	0.8568	0.8302	0.8693	0.7022	6.9885
24	250	8	256	0.9382	0.9397	0.9372	0.9219	0.8658	0.8364	0.8698	0.6929	7.0019
25	250	8	512	0.9391	0.9384	0.9361	0.9216	0.8677	0.8300	0.8772	0.7019	7.0120
26	250	8	1024					OOM				

Table 8: The fine-tuning results of GL-based foundation models.

Case	Windows	Depth	Dims	AUROC				AUPRC				Criteria
				MI	STTC	CD	HYP	MI	STTC	CD	HYP	
0	60	2	256	0.9408	0.9335	0.9352	0.9198	0.8644	0.8164	0.8660	0.6910	6.9671
1	60	2	512	0.9384	0.9318	0.9352	0.9168	0.8619	0.8126	0.8686	0.6962	6.9615
2	60	2	1024	0.9353	0.9333	0.9368	0.9143	0.8542	0.8134	0.8657	0.6895	6.9425
3	60	4	256	0.9411	0.9351	0.9329	0.9128	0.8710	0.8207	0.8633	0.6698	6.9467
4	60	4	512	0.9300	0.9377	0.9367	0.9180	0.8464	0.8188	0.8697	0.6839	6.9412
5	60	4	1024	0.9365	0.9370	0.9360	0.9066	0.8629	0.8261	0.8644	0.6790	6.9485
6	60	8	256	0.9379	0.9349	0.9396	0.9196	0.8601	0.8246	0.8743	0.6999	6.9909
7	60	8	512	0.9390	0.9353	0.9333	0.9151	0.8653	0.8172	0.8653	0.6815	6.9520
8	60	8	1024	0.9364	0.9330	0.9364	0.9150	0.8588	0.8167	0.8675	0.6795	6.9433
9	125	2	256	0.9387	0.9385	0.9337	0.9167	0.8626	0.8317	0.8678	0.6801	6.9698
10	125	2	512	0.9389	0.9420	0.9362	0.9191	0.8665	0.8350	0.8753	0.6960	7.0090
11	125	2	1024	0.9427	0.9393	0.9400	0.9185	0.8728	0.8295	0.8740	0.6814	6.9982
12	125	4	256	0.9404	0.9361	0.9361	0.9137	0.8671	0.8223	0.8695	0.6713	6.9565
13	125	4	512	0.9396	0.9360	0.9363	0.9195	0.8649	0.8261	0.8714	0.7042	6.9980
14	125	4	1024	0.9387	0.9370	0.9369	0.9157	0.8683	0.8222	0.8737	0.6852	6.9777
15	125	8	256	0.9393	0.9359	0.9376	0.9220	0.8637	0.8176	0.8744	0.6791	6.9696
16	125	8	512	0.9330	0.9412	0.9367	0.9178	0.8551	0.8352	0.8725	0.6910	6.9825
17	125	8	1024	0.9410	0.9370	0.9344	0.9095	0.8714	0.8274	0.8646	0.6903	6.9756
18	250	2	256	0.9369	0.9390	0.9380	0.9230	0.8643	0.8347	0.8787	0.6941	7.0087
19	250	2	512	0.9346	0.9349	0.9348	0.9214	0.8576	0.8178	0.8742	0.6932	6.9685
20	250	2	1024	0.9346	0.9373	0.9389	0.9117	0.8562	0.8299	0.8713	0.6695	6.9494
21	250	4	256	0.9379	0.9346	0.9368	0.9183	0.8696	0.8217	0.8733	0.6779	6.9701
22	250	4	512	0.9346	0.9338	0.9358	0.9249	0.8542	0.8195	0.8720	0.6931	6.9679
23	250	4	1024	0.9409	0.9370	0.9365	0.9259	0.8703	0.8236	0.8691	0.6957	6.9990
24	250	8	256	0.9387	0.9326	0.9393	0.9272	0.8694	0.8182	0.8762	0.6930	6.9946
25	250	8	512	0.9377	0.9359	0.9441	0.9125	0.8600	0.8279	0.8854	0.6800	6.9835
26	250	8	1024	0.9409	0.9403	0.9350	0.9097	0.8684	0.8404	0.8699	0.6838	6.9884

Table 9: The fine-tuning results of HL-based foundation models.

Case	Windows	Depth	Dims	AUROC				AUPRC				Criteria
				MI	STTC	CD	HYP	MI	STTC	CD	HYP	
0	60	2	256	0.9418	0.9413	0.9364	0.9257	0.8732	0.8366	0.8736	0.7018	7.0304
1	60	2	512	0.9446	0.9400	0.9400	0.9291	0.8814	0.8435	0.8778	0.7023	7.0587
2	60	2	1024	0.9444	0.9398	0.9360	0.9237	0.8786	0.8354	0.8742	0.6966	7.0287
3	60	4	256	0.9444	0.9364	0.9378	0.9274	0.8753	0.8236	0.8775	0.6976	7.0200
4	60	4	512	0.9472	0.9376	0.9399	0.9254	0.8810	0.8337	0.8826	0.6951	7.0425
5	60	4	1024	0.9427	0.9398	0.9365	0.9257	0.8746	0.8365	0.8788	0.6975	7.0321
6	60	8	256	0.9434	0.9434	0.9428	0.9291	0.8779	0.8389	0.8847	0.7003	7.0605
7	60	8	512	0.9453	0.9368	0.9366	0.9339	0.8828	0.8331	0.8766	0.7104	7.0555
8	60	8	1024					OOM				
9	125	2	256	0.9434	0.9396	0.9415	0.9234	0.8803	0.8339	0.8807	0.6948	7.0376
10	125	2	512	0.9406	0.9412	0.9391	0.9213	0.8735	0.8365	0.8796	0.6881	7.0199
11	125	2	1024	0.9452	0.9403	0.9425	0.9245	0.8799	0.8363	0.8835	0.6988	7.0510
12	125	4	256	0.9432	0.9370	0.9408	0.9252	0.8747	0.8315	0.8806	0.7027	7.0357
13	125	4	512	0.9448	0.9398	0.9449	0.9307	0.8809	0.8339	0.8841	0.7153	7.0744
14	125	4	1024	0.9461	0.9417	0.9390	0.9219	0.8828	0.8400	0.8794	0.6948	7.0457
15	125	8	256	0.9434	0.9413	0.9399	0.9163	0.8749	0.8373	0.8820	0.6824	7.0175
16	125	8	512	0.9433	0.9378	0.9446	0.9207	0.8782	0.8271	0.8867	0.6772	7.0156
17	125	8	1024					OOM				
18	250	2	256	0.9442	0.9406	0.9428	0.9253	0.8773	0.8412	0.8837	0.6960	7.0511
19	250	2	512	0.9418	0.9390	0.9410	0.9240	0.8737	0.8289	0.8835	0.6962	7.0281
20	250	2	1024	0.9435	0.9366	0.9381	0.9202	0.8788	0.8277	0.8715	0.6964	7.0128
21	250	4	256	0.9413	0.9394	0.9432	0.9256	0.8758	0.8399	0.8846	0.6979	7.0477
22	250	4	512	0.9437	0.9406	0.9415	0.9215	0.8791	0.8428	0.8823	0.6890	7.0405
23	250	4	1024	0.9452	0.9393	0.9393	0.9203	0.8800	0.8375	0.8773	0.6811	7.0200
24	250	8	256					OOM				
25	250	8	512					OOM				
26	250	8	1024					OOM				